Application of Density Functional Theory and Vibrational Spectroscopy Toward the Rational Design of Ionic Liquids

Sergey A. Katsyuba,*,† Elena E. Zvereva,† Ana Vidiš,‡ and Paul J. Dyson‡

A. E. Arbuzov Institute of Organic and Physical Chemistry, Kazan Scientific Centre of the Russian Academy of Sciences, Arbuzov Street 8, 420088 Kazan, Russia and Institut des Sciences et Ingénierie Chimiques, Ecole Polytechnique Fédérale de Lausanne (EPFL), CH−1015 Lausanne, Switzerland

Received: July 20, 2006; In Final Form: October 20, 2006

Density functional theory methods in combination with vibrational spectroscopy are used to investigate possible variants of molecular structure of the ion pairs of several imidazolium-based ionic liquids (ILs). Multiple stable structures are determined with the anion positioned (a) near to the C2 atom of the imidazolium ring, (b) between N1 and C5, (c) between N3 and C4, and (d) between C4 and C5. Chloride and bromide anions in vacuum also occupy positions above or below the imidazolium ring, but in the condensed state these positions are destabilised. In comparison with the halides that almost equally occupy the positions (a−d), tetrafluoroborate and hexafluorophosphate anions strongly prefer position (a). The position and the type of the anion influence the conformation of the side chains bound to the imidazolium N1 atom, which are able to adopt in vacuum all usual staggered or eclipsed conformations, although in the liquid state some of the conformations are present only as minor forms if at all. Vibrations of the cations depend both on the conformational changes and on the association with the anion. The formation of the ion pairs influences mainly stretching and out-of-plane vibrations of the imidazolium C−H groups and stretching vibrations of the perfluoroanions. Other modes of the ions retain their individuality and practically do not mix. This allows "interionic" vibrations to be separated and to regard the couple of the ions as an anharmonic oscillator. Such a model correlates the molecular structure of various ILs and their melting points without involving the energy of the interaction between the cations and anions but explains structure-melting point correlations on the grounds of quasy-elastic properties.

Introduction

Room-temperature ionic liquids (ILs) are typically composed of organic cations (e.g., 1-alkyl-3-methyl-imidazolium, see Chart 1) and inorganic anions (e.g., chloride, tetrafluoroborate, or hexafluorophosphate). Unlike inorganic molten salts such as NaCl, they are fluid at or near room temperature. Interest in ILs has increased considerably over the past few years, fueled by the development of new synthetic routes to ILs and the preparation of new ILs, together with an increasing range of potential applications.[1] Notably, with the discovery of the air and moisture stable imidazolium based ILs,[2] the field has developed at an incredible rate with particular focus on the use of ILs as reaction media for stoichiometric organic synthesis and catalysis, as electrolytes in solar cells, and in analytical processes.[3] ILs are perceived to be environmentally benign, largely because they are nonvolatile, but they have other intriguing properties such as high thermal stability, high loading capacity, and tuneable solvent properties.[4] Through different combinations of cations and anions, there is a tremendous variety of "designer" solvents.[5] However, to a large extent the process of design remains a random event as the features that control the physical properties of ILs remain poorly understood.

To rationalize interrelations between structure and properties of ILs, reliable data on the structure and bonding in ionic liquids are needed. Because X-ray structural elucidation of liquids is not routinely feasible, it is necessary to rely on spectroscopic methods. Vibrational spectroscopy is widely used in studies of ILs for several reasons: (i) Internal rotation of various conformationally flexible groups of both cations and anions or possible movements of anions relative to cations are slow on the infrared (IR) and Raman spectroscopic timescales. As a result, all possible isomers are observable as separate species, and their spectra are not averaged. (ii) Hydrogen bonding is most straightforwardly exhibited in IR spectra. For example, the so-called "Cl^- interaction band" at ca. 3050 cm^{-1}, which is

CHART 1: Numbering Scheme for Imidazolium-Based Ionic Liquids

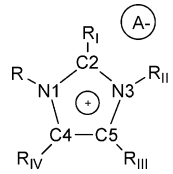

1 R = Et (C6−C7), R_I = H, R_{II} = Me, R_{III} = R_{IV} = H, *A* = Cl; **2** R = Et, R_I = H, R_{II} = Me, R_{III} = R_{IV} = H, *A* = Br; **3** R = Et, R_I = H, R_{II} = Me, R_{III} = R_{IV} = H, *A* = I; **4** R = Bu (C6−C7-C8−C9), R_I = H, R_{II} = Me, R_{III} = R_{IV} = H, *A* = Cl; **5** R = Me, R_I = H, R_{II} = Me, R_{III} = R_{IV} = H, *A* = Cl; **6** R = Et, R_I = H, R_{II} = Me, R_{III} = R_{IV} = H, *A* = BF_4; **7** R = Bu, R_I = H, R_{II} = Me, R_{III} = R_{IV} = H, *A* = BF_4; **8** R = iPr, R_I = H, R_{II} = iPr, R_{III} = R_{IV} = Me, *A* = BF_4; **9** R = Me, R_I = H, R_{II} = Me, R_{III} = R_{IV} = H, *A* = BF_4; **10** R = Et, R_I = Me, R_{II} = Me, R_{III} = R_{IV} = H, *A* = BF_4; **11** R = Pr (C6−C7-C8), R_I = H, R_{II} = Me, R_{III} = R_{IV} = H, *A* = BF_4; **12** R = All (C6−C7 = C8), R_I = H, R_{II} = Me, R_{III} = R_{IV} = H, *A* = BF_4; **13** R = Et, R_I = H, R_{II} = Me, R_{III} = R_{IV} = H, *A* = PF_6

* Corresponding author. E-mail: skatsyuba@yahoo.com. Tel: +7 8432 7318 92. Fax: +7 8432 7322 53.
† Kazan Scientific Centre of the Russian Academy of Sciences.
‡ Ecole Polytechnique Fédérale de Lausanne (EPFL).

10.1021/jp064610i CCC: $37.00
Published on Web 12/19/2006

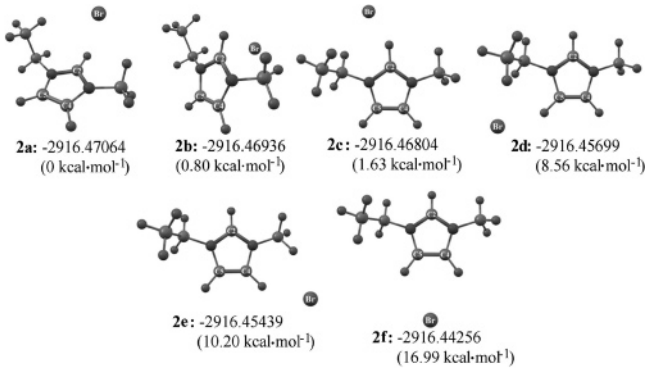

Figure 1. Stable structures of [EMIM]Br, their B3LYP/6-31G* (Hartree) electronic energies, and their energies relative to the global-minimum energy (in parenthesis): **2a**, top; **2b**, bottom; **2c**, forward; **2d**, ethside; **2e**, methside; **2f**, back (see text for nomenclature). These structures, computed in this work, are similar to the stable [EMIM]Cl, [EMIM]Br and [BMIM]Cl structures found in refs 9 and 10.

assigned to stretching vibrations of C2−H, C4−H and C5−H hydrogen-bonded to the chloride anion, has been observed in the IR spectra of 1-ethyl-3-methylimdazolium chloride [EMIM]-Cl (**1**) in both the solid and the liquid states.[6] A combined crystallographic−IR spectroscopic study[7] confirmed that the chloride was located in hydrogen bond positions C2−H, C4−H and C5−H, characteristic of C−H...Cl^- interactions. Similar Br^- and I^- interaction bands are also found between 3050 and 3080 cm^{-1} in the spectra of EMIM bromide (**2**) and iodide (**3**).[8] According to X-ray data,[8] the local structure around the EMIM cation is similar to that observed for **1**. Namely, each cation is H-bonded via C2−H, C4−H and C5−H bonds to three anions, lying approximately in the plane of the ring. Ab initio HF and MP2 computations[9] for **1**−**3** demonstrate that these three positions of the halogen correspond to local minima on the potential energy surface of the isolated ion pairs (structures **2c**−**e** in Figure 1).

Of these three local minima the one (**2c**) with the halogen positioned to interact with the most acidic proton, viz. H−C2, generally has the lowest energy. The global minimum **2a** corresponds to the halogen positioned over the ring in a close proximity to H−C2. A thorough quantum chemical study[10] of 1-butyl-3-methylimdazolium chloride [BMIM]Cl (**4**) exploiting desnity functional theory (DFT) and ab initio MP2 and CCSD-(T) levels of theory revealed that there are four associates in which the chloride remains roughly in-plane with the imidazolium ring (similar to **2b**−**e** in Figure 1) and one in which the chloride lies above the plane of imidazolium ring, and more specifically above the C2−H bond (similar to **2a** in Figure 1). Molecular dynamic simulations[11,12] and neutron diffraction studies[13,14] of the melts of **1** and 1,3-dimethylimdazolium chloride [DMIM][Cl] (**5**) also locate the Cl^- ion in both the plane of the ring and in out-of-the plane positions. However, ab initio molecular dynamics (MD) simulations of **5**[15,16] show significant differences to both the classical calculations[12] and neutron studies:[14] the chloride ions tend to be located in the plane of the imidazolium ring in the above mentioned hydrogen bond positions, as in the crystal,[17] instead of occupying the position over the ring. Evidence for the H-bonding not only in the liquid state, but also in solutions of EMIM halides, also has been obtained from multinuclear NMR spectroscopy and conductivity measurements.[18]

Reports from Hamaguchi's group[19−21] have investigated how the $BMIM^+$ cation interacts with a number of different anions using Raman spectroscopy, and the polymorphism observed in the chloride salt, **4**, has been independently verified by two groups.[19,22−24] The $BMIM^+$ cations were found to differ in their conformation in the two polymorphs. In the monoclinic form, the butyl chain is all *anti*, and in the orthorhombic form the chain is *gauche* around C7−C8 (see Chart 1 for numbering of atoms). Vibrational analysis based on DFT calculations[19] indicate that several Raman bands could be used as markers for the rotational isomerism around the C7−C8 bond of the n-butyl group. A similar approach based on ab initio MP2 computations and Raman spectroscopy revealed that coexistence of the above mentioned *anti* and *gauche* forms is a general feature of the long-chain 1-alkyl derivatives of imidazolium based ILs.[25]

The possibility of internal rotation of the ethyl group in $EMIM^+$ about the N−C bond was analyzed by Umebayashi et al.[26] A Camridge Structural Database search combined with HF, MP2, and B3LYP computations revealed that the EMIM cation was able to exist in two conformations both in the crystalline state and in vacuum. The two conformers correspond to those with a planar and nonplanar ethyl group relative to the imidazolium ring plane, the nonplanar conformer being considerably more favored. An "extra" band in the Raman spectra of the $EMIM^+$ cation with a number of different anions was assigned to the minor planar conformer.[26]

It is noteworthy that these two conformations may be regarded only for the isolated $EMIM^+$ cation. Introduction of a counterion in an out-of-plane position, relative to the imidazolium ring, gives rise to the possibility of two nonplanar conformers: (a) with the ethyl group and the counterion on the same side relative to the plane of the imidazolium ring, and (b), with the ethyl group and the counterion on the opposite sides relative to the plane of the imidazolium ring. Unlike the chloride systems in which the chloride was found in the plane of the ring, BF_4^- and PF_6^- are mostly positioned over the ring[27−38] and have short contacts not only with H−C(2), but also with protons of alkyl groups. HF, MP2, and B3LYP computations[31,32] of [AlkMIM][BF_4] and [AlkMIM][PF_6] (Alk = Me, Et, Pr, Bu) demonstrate that the conformations of type (a) are more energetically stable in vacuum than the type (b) conformations. Consequently, three different conformations (one planar and two nonplanar) of the $EMIM^+$ cation should be expected to exist in the [EMIM][BF_4] (**6**) ion pair, although only two of the above mentioned nonplanar conformers (a) and (b) were regarded by Tsuzuki et al.[31] Nevertheless, the overall number of minima found on the potential energy surface of **6** amounted to nine.[31] The global minimum corresponded to structure **6a** shown in Figure 2. Four further structures, **6b**−**e**, are very similar to it; merely the conformation of the ethyl group and the orientation of the B−F bonds differ. The energies of these five minima were much lower than the energies of another four structures (**6f**, **6g**, **6i**, **6m** in Figure 2). The global minimum corresponds to the major form of **6** in the liquid state,[29] but in the crystal structure of [EMIM][BF_4] the compound adopts the structure close to that of structure **6h**.[38] This latter structure, as well as other structures **6c**−**g** and **6f**−**m** (Figure 2), were not taken into account by Carper et al.[30,32] during their simulations of the vibrational spectra of the isolated ion pairs [AlkMIM][BF_4] and [AlkMIM][PF_6]. Only two or three conformations were regarded for every [AlkMIM][BF_4] ion pair,[32] and the vibrations of only one nonplanar conformer were calculated for corresponding ion pairs containing the hexafluorophosphate anion.[30] No clear manifestations of conformational inhomogeneity have been found in the vibrational spectra of [AlkMIM][BF_4][32] and [AlkMIM][PF_6],[30] except for *gauche*−*anti* transitions around the C7−C8 bond in [BMIM][BF_4] (**7**).[32]

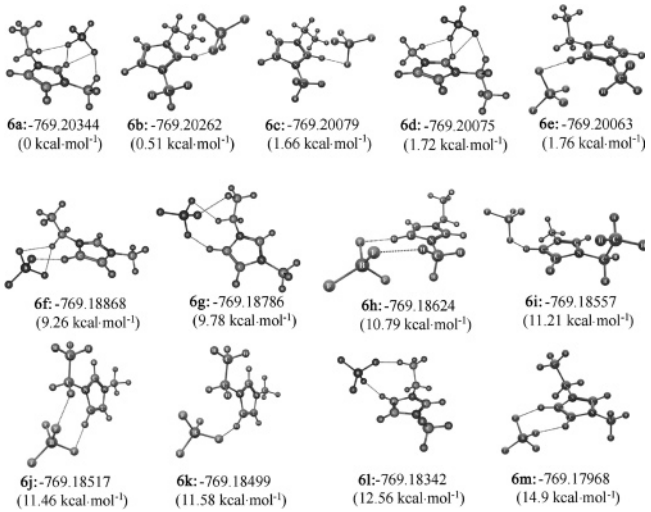

Figure 2. Stable [EMIM][BF_4] structures, their B3LYP/6-31G* (Hartree) electronic energies, and their energies relative to the global-minimum energy (in parenthesis). Short contacts between F and H atoms are indicated with dotted lines. **6a**−**6e**, forward; **6f**, **6g**, and **6j**−**6l**, ethside; **6h** and **6i**, methside; **6m**, back (see text for nomenclature). These structures, computed in this work, are similar to the stable [EMIM][BF_4] structures found in ref 31.

Compared to the halides **1**-**5** that have been thoroughly studied, less is known about the capacity of imidazolium tetrafluoroborates and hexafluorophosphates to form hydrogen bonds. The IR[29,39] and Raman[29] spectra of **6** and **7** exhibit two aromatic C−H stretching bands at ca. 3170 and ca. 3125 cm^{-1}. The latter is ascribed[29,39] to hydrogen bonding between C2-H and BF_4^- with this assignment being supported by quantum chemical computations.[29] The structural criteria for H-bond formation are not clearly defined. For example, according to X-ray data[40] obtained on a single crystal of 1,3-diisopropyl-4,5-dimethylimidazolium tetrafluoroborate (**8**), the BF_4^- anion is localized in the plane of the ring and has a moderately close contact with H-C2. Simultaneously, the (C2)H...F distance is about 0.1 Å longer than the distance between another fluorine atom of the tetrafluoroborate anion and a proton of isopropyl moiety of the second neighboring cation. Thus, it is not quite clear whether hydrogen bonding is present in 1-alkyl-3-methylimidazolium tetrafluoroborates or whether the short contacts have another origin. In any case, these weak H-bonds are not essential for the attraction between the ions that keeps the cations and anions closely associated[29,31] even in CD_2Cl_2.[29]

The overall conclusions from these wealth of studies are that there is some evidence for the presence of conformers in the liquid state, and that 1-alkyl-3-methylimidazolium cations tend to form multiple, short contacts to counterions. For the halides, the short contacts can be regarded as hydrogen bonds with the participation of H(2), H(4), H(5), and possibly some other protons of the cation. For weak H-bond acceptors such as tetrafluoroborate and hexafluorophosphate, the character of their contacts and the specific points on the cation where interactions with counterions occur, still remain unclear. It therefore seems of interest (1) to carry out a complete conformational analysis of various imidazolium-based systems and to see whether the conformers were confined to internal rotation around the C7−C8 or N-alkyl bonds or to a more general phenomenon and (2) to explore how different anions influence the structure of associates in ILs and their mode of binding.

Vibrational spectroscopy is a versatile tool for probing conformations and H-bonding of both liquid and solid materials and their solutions. Accordingly, in this paper we present results from IR and Raman spectroscopic experiments as well as DFT calculations of the structure and vibrational modes of halides, tetrafluoroborates, and hexafluorophosphate based imidazolium salts. As will be discussed, the computations are used to predict possible variants of molecular structure and to simulate vibrational spectra for all these variants. The simulations followed by comparisons of the computational predictions with the experimental spectroscopic data allow complete interpretation of the IR and Raman spectra and allow conclusions regarding the mutual orientation of the anions and cations, conformations of the latter, their hydrogen bonding, etc. After elucidation of these structural features, we analyze their influence on the melting points of ILs within the framework of a simple theoretical model of an anharmonic oscillator.

Experimental Section

Ionic liquids were prepared according to literature procedures.[2] Prior to use, all of the ionic liquids were dried for 24 h, and all samples preparations were carried out in a glove box with the exclusion of moisture. Differential scanning calorimetry was performed using a SETARAM DSC 131. The temperature peaks are associated with 2° phase transition upon cooling and warming. CD_2Cl_2 was purchased from ARMAR AG and used without further purification. All solution preparations were carried out in a glove box with the exclusion of moisture. IR spectra were recorded on a Perkin-Elmer FT−IR 2000 spectrometer between 400 and 4000 cm^{-1} and a Bruker IFS 113v FT−IR spectrometer in the range 200−650 cm^{-1} at a resolution of 1 cm^{-1}. Liquid samples were prepared as thin films between KBr or BaF_2 plates. Spectra of CD_2Cl_2 solutions were recorded in 0.27 mm NaCl cells. The concentrations were ca. 10^{-1} M. Raman spectra were recorded on a Coderg PHO-82 spectrometer with a double monochromator using a He−Ne laser (LG-36A, $\lambda = 632.8$ nm, power 30 mW). FT Raman spectra were recorded on a BRUKER RAM II module (using a Ge detector) attached to a BRUKER VERTEX 70 FTIR spectrometer. The COMPASS 1064-500 diode laser pumped Nd:YAG with a wavelength of 1064 nm (power of 50 mW) was used as a source of excitation. The samples were placed in standard glass capillaries.

Computations. All ab initio calculations were carried out using the Gaussian-98 and Gaussian-03 suites of programs.[41] For DFT, Becke's three-parameter exchange functional[42] was used in combination with the Lee−Yang−Parr correlation functional[43] (B3LYP) and standard 6-31G* basis set. All stationary points were characterized as minima by analysis of the Hessian matrices. The calculated force fields were transformed to internal coordinates, and the scaling procedure was applied using the program described in ref 44. The reason being that although DFT produces rather accurate vibrational frequencies, even these computations show systematic errors mainly due to limited basis sets, harmonic approximation and remaining deficiencies in describing electron correlation. Transferable scaling factors compensate for most of these errors.[45] It has been demonstrated earlier that the scaled quantum mechanical (SQM) method allowed a priori quantitative prediction of the IR and Raman spectra of various molecules, including the atoms H, B, C, N, O, F, P, S, and Cl.[29,46−48] The transferable scaling factors employed in this work are summarized in Supporting Information, Table 1S.

Results and Discussion

Computed Structures. The optimized structures of the [EMIM] ion pairs with the halides can be classified according to the primary cation−anion interactions shown in Figure 1.

TABLE 1: Vibrational Spectra of [EMIM][BF_4]

Experiment (liquid)		Computations [ν, cm^{-1c} (I_{IR}, km/mole; I_{Ra}, Å4/AMU/ρ)]			Assignments
IR (ν/cm^{-1}, I^a)	Raman (ν/cm^{-1}, I, ρ^b)	**6a**	**6h**	**6j**	**6a**[d]
3166 s	3172 w, 0.63	3178 (1; 100/ 0.13)	3170 (0; 95/ 0.20)	3187 (9; 45/ 0.36)	νC4-H,C5-H (in-phase)
		3161 (4; 51/ 0.80)	3167 (13; 17/ 0.61)	3169 (5; 75/ 0.41)	νC4-H,C5-H (out-of-phase)
3125 s−m	3122 vw, dp?	3135 (244; 46/ 0.29)			ν C2-H
	3112 vw, dp?				
			2999 (454; 110/ 0.25)		ν C4-H
				2978 (507; 165/ 0.35)	ν C5-H
2989 m−w		3007 (14; 41/ 0.83)	3022 (11; 69/ 0.64)	3042 (4; 53/ 0.85)	ν_{as} CH_3 (Me)
		2995 (0; 14/ 0.55)	3018 (107; 81/ 0.60)	3010 (27; 43/ 0.85)	ν_{as} CH_3, CH_2
~2970 w sh	2971 m, 0.42	2984 (1; 54/ 0.70)	2972 (16; 5/ 0.68)	2992 (5; 82/ 0.86)	ν_{as} CH_3, CH_2
		2982 (9; 75/ 0.82)	2964 (22; 107/ 0.58)	2964 (19; 105/ 0.63)	ν_{as} CH_3 (Me)
2952 w	2946 m, 0.5	2949 (22; 96/ 0.60)	2950 (0; 91/ 0.75)	2948 (7; 75/ 0.24)	ν_{as} CH_3 (Et)
				2931 (30; 62/ 0.84)	ν_{as} CH_3 (Et)
~2917 vvw	2928 w	2913 (32; 117/ 0.21)	2914 (16; 82/ 0.11)	2916 (24; 160/ 0.06)	ν_s CH_2
		2905 (36; 152/ 0.07)	2910 (49; 148/ 0.02)		ν_s CH_3 (Me)
2892 vw	2887 w	2885 (26; 109/ 0.06)	2892 (9; 122/ 0.02)	2874 (22; 111/ 0.02)	ν_s CH_3 (Et)
1619 sh	1606 vw				
1576 s	1569 m, dp?	1583 (17; 4/ 0.41)	1597 (55; 1/ 0.43)	1593 (50; 1/ 0.53)	ν C═C
1571 s sh		1571 (51; 2/ 0.69)	1567 (35; 2/ 0.67)	1575 (38; 2/ 0.63)	ν_{as} N1C2N3, r C2H
1462 m		1475 (5; 7/ 0.75)	1468 (47; 15/ 0.70)	1491 (2; 19/ 0.84)	δ_{as} CH_3 (Et)
		1472 (8; 21/ 0.77)	1466 (15; 9/ 0.58)	1471 (6; 10; 0.85)	δ_{as} CH_3 (Me)
1458 m	1453 m, dp	1465 (12; 15/ 0.71)	1460 (13; 21/ 0.75)	1468 (9; 18; 0.86)	δ_{as} CH_3 (Me)
		1460 (11; 9/ 0.73)	1446 (6; 23/ 0.74)	1457 (22; 24/ 0.84)	δ CH_2
		1448 (2; 29/ 0.71)	1445 (4; 14/ 0.72)	1447 (11; 18/ 0.86)	δ_{as} CH_3 (Et)
1432 vw	1422 s, 0.28	1431 (11; 16/ 0.77)	1430 (13; 14/ 0.75)	1436 (5; 12/ 0.82)	δ_s CH_3
		1424 (4; 28/ 0.24)	1411 (6; 13/ 0.28)	1420 (30; 15/ 0.37)	δ CH_2, ν ring
1392 w	1389w	1396 (12; 3/ 0.51)	1390 (5; 4/ 0.43)	1389 (12; 4/ 0.59)	δ_s CH_3 (Et), w CH_2
		1384 (2; 9/ 0.15)	1372 (8; 20/ 0.14)	1385 (9; 13/ 0.29)	ν_{as} C2N1C5, $\delta_s$$CH_3$(Et)
1358 vw	1346 sh	1360 (7; 1/ 0.74)	1365 (17; 3/ 0.70)	1347 (19; 24/ 0.27)	w CH_2
1337 w	1334 s, 0.47	1315 (10; 24/ 0.34)	1326 (24; 34/ 0.33)	1316 (27; 15/ 0.62)	ν N−Et, N−Me, breathing
~1300 w sh	1296 w	1293 (2; 2/ 0.63)	1307 (2; 5/ 0.56)	1299 (4; 8/ 0.76)	r C4-H, C5-H, t CH_2
1286 m		1259 (473; 0/ 0.45)	1235 (471; 0/ 0.31)	1235 (523; 1/ 0.40)	ν BF_4
1250 vvw	1254 w	1256 (8; 3/ 0.67)	1256 (2; 5/ 0.68)	1269 (19; 7/ 0.79)	r *C*2-H
1172 s	1170 w, dp	1157 (173; 2/ 0.71)	1166 (172; 2/ 0.70)	1158 (110; 6/ 0.66)	r 2-H, rC4-H,ν N−Et, N−Me
1120 sh	1116 m, dp	1144 (26; 4/ 0.54)	1140 (40; 1/ 0.62)	1137 (36; 1/ 0.86)	r CH_3
		1133 (4; 2/ 0.25)	1130 (5; 2/ 0.75)	1132 (1; 2/ 0.82)	r CH_2, r CH_3 (Et)
				1130 (14; 3/ 0.84)	r CH_3, r C4-H, r C5-H
[e]		1103 (17; 4/ 0.33)	1113 (1; 3/ 0.47)		r CH_3
[e]	1088 s, 0.44	1092 (6; 4/ 0.53)	1101 (1; 2/ 0.43)	1093 (9; 9/ 0.83)	r C−H
[e]		1088 (11; 6/ 0.38)	1081 (4; 3/ 0.15)	1081 (18; 7/ 0.18)	r CH_3
[e]		1070 (207; 1/ 0.83)	1074 (258; 1/ 0.31)	1077 (230; 1/ 0.46)	ν BF_4
[e]	1033 sh	1041 (41; 2/ 0.69)	1066 (225; 1/ 0.62)	1061 (167; 2/ 0.57)	δ ring
[e]	1026 s, 0.45	1019 (32; 8/ 0.17)	1028 (26; 5/ 0.3)	1026 (11; 6/ 0.21)	breathing, νN−Et, νN−Me
		997 (83; 2/ 0.22)	1003 (78; 9/ 0.17)	1003 (132; 2/ 0.85)	ν BF_4
985 vw					
960 w	961 m, 0.55	939 (3; 6/ 0.33)	937 (1; 7/ 0.38)	950 (11; 5/ 0.24)	ν CC (Et)
935 vw sh					
912 vw		985 (181; 1/ 0.82)			γ C−H
896 w			890 (4; 1/ 0.57)	893 (2; 1/ 0.71)	γ C−H
	861 w, dp				
849 m					
		811 (0; 0/ 0.81)	788 (1; 0/ 0.61)	764 (8; 0/ 0.83)	γ C−H
805 w	804 vw, dp	804 (12; 0/ 0.53)	786 (36; 0/ 0.56)	791 (34; 1;0.86)	r CH_2, r CH_3 (Et)
758 m	765 vs, 0.13	758 (10; 3/ 0.03)	760 (9; 3/ 0.03)	759 (9; 3/ 0.06)	ν_s BF_4
		722 (28; 2/ 0.85)	720 (4; 1/ 0.70)	722 (5; 1/ 0.78)	γ C−H
702 w	701 m, 0.88	692 (12; 2/ 0.72)	689 (1; 3/ 0.73)	699 (0; 4/ 0.74)	ν N−Me, ν N−Et
649 m	649 vw, 0.74	671 (37; 0/ 0.69)	643 (13; 0/ 0.66)		γ N−Et, γ N−Me, ring-packering
		659 (31; 1/0.77)	641 (12; 0/0.75)		
623 m	624 w, dp	627 (3; 1/ 0.73)	627 (5; 0/ 0.73)	629 (9; 0/ 0.76)	γ N−Me, ring-packering
				609 (7; 0/ 0.86)	γ N−Me, ring-packering
				616 (9; 0/0.86)	
598 w	599 vs, 0.39	589 (1; 6/ 0.25)	585 (1; 5/ 0.22)	580 (1; 5/ 0.37)	ν N−Et, ν N−Me
		525 (21; 1/ 0.83)	528 (21; 1/ 0.75)	527 (19; 1/ 0.86)	δ BF_4
521 w	520 m, dp	515 (3; 0/ 0.47)	517 (3; 0/ 0.75)	516 (3; 0/ 0.86)	δ BF_4, ν BF_4
		511 (2; 0/ 0.86)	511 (2; 0/ 0.75)	512 (2; 0/ 0.85)	δ BF_4, ν BF_4
	475 w				
423 vw	438 m, br 0.75	437 (2; 1/ 0.33)	443 (5; 1/ 0.65)	449 (3; 3/ 0.67)	r N−Et, r N−Me
404 vw					
381 vw sh	381 m-w, dp	387 (2; 1/ 0.46)	382 (3; 2/ 0.18)		δ NEt
				368 (1; 0/ 0.26)	δ NEt

TABLE 1: Continued

Experiment (liquid)		Computations [ν, cm^{-1c} (I_{IR}, km/mole; I_{Ra}, Å4/AMU/ρ)]			Assignments
IR (ν/cm^{-1}, I^a)	Raman (ν/cm^{-1}, I, ρ^b)	**6a**	**6h**	**6j**	**6a**^{d}
354 vw	351 w, dp	357 (0; 0/ 0.84)	366 (1; 0/ 0.75)	356 (1; 0/ 0.64)	δ BF_4
		352 (0; 0/ 0.80)	349 (1; 0/ 0.75)	349 (0; 0/ 0.82)	δ BF_4
294 vw	286 vw, dp	304 (1; 0/ 0.73)	308 (4; 0/ 0.44)	291 (0; 0/ 0.81)	tors CH_3 (Et)
243 vw	241 m, dp	242 (2; 1/ 0.8)	239 (2; 1/ 0.67)	241 (0; 1/ 0.86)	γ N−Me, ring-packering

[a] w, weak; m, medium; s, strong; v, very; sh, shoulder; br, broad. [b]Depolarisation ratio; dp, depolarised. [c]SQM scaled wavenumbers. [d]ν, stretch; δ, bend; w, wagging; t, twisting; r, rocking; γ, out-of-plane; s, symmetrical; as, antisymmetrical. [e]Absorption at about 100%.

There are four associations in which the halide remains roughly in-plane with the imidazolium ring (**2c**−**f**) and two in which the halide lies above (**2a**) or below (**2b**) the plane of imidazolium ring with respect to the orientation of the ethyl group. The results for [EMIM]Cl essentially coincide with the results published by Hunt and Gould for [BMIM]Cl.[10] In the case of (**2**), we have found three local minima (**2b**, **2d**, and **2f** in Figure 1) in addition to four structures (**2a** and mirror images of **2a**, **2c**, and **2e**) previously found by Turner et al.[9] As a result, the distribution of local minima, corresponding to possible orientations of the anion relative to the cation, coincides qualitatively for both halides.

Herein, following the classification proposed by Hunt and Gould,[10] the structures shown in Figure 1 will be identified as "front" (**2c**, interaction through C2−H), "top" (**2a**, anion above the imidazolium ring), "bottom" (**2b**, anion below the imidazolium ring) "ethside" (**2d**, positioned between N1 and C5), "methside" (**2e**, positioned between N3 and C4), and "back" (**2f**, positioned between C4 and C5). These sites can be linked to the density maps produced from MD simulations.[11,12] The computed front, ethside, methside, and back structures have been found in the crystal structures of EMIM and other AlkMIM halides; the top and bottom isomers have not been observed in any crystal structure. Ab initio MD simulations of **5**[15,16] show that the structures with the shortest contacts between counterions are very similar between liquid and solid states. Thus, the top and bottom structures seem to be destabilised not only by crystal packing effects but also in the liquid state.

We have tried to evaluate the influence of the surrounding medium on the relative stability of the top (bottom) and forward structures within the framework of the polarized continuum model (PCM).[49] The model employs a self-consistent reaction field (SCRF) methodology for modeling systems in solution. Several parameters of the simulated solution, such as dielectric constant, are needed for the PCM computations. Because these parameters for the EMIM halides are not available, a solution of **2** in CH_2Cl_2 was simulated. It is known that in this solution **2** exists in a quasi-molecular state.[18] Thus, treating **2** diluted in CH_2Cl_2 as an isolated ion pair, placed in a polarizable continuum, may be regarded as a reasonable approximation. Optimization of the structures **2a** and **2b** demonstrated that these top and bottom associations do not correspond to minima in the liquid state. The global minimum structure of **2** in CH_2Cl_2 is the forward structure **2c**. Methside and ethside structures are less energetically stable, but the energy gaps between the minima (about 1 kcal/mol) are small compared to the case of **2** isolated in vacuum (Figure 1). These small energy differences agree well with the experimental observation[18] in that the EMIM cation forms strong hydrogen bonds with bromide, using all three ring protons H2, H4, and H5, which means that both forward and back and/or side minima are populated.

Optimized structures of the tetrafluoroborates [MMIM][BF_4] (Figure 3), [EMIM][BF_4] (Figure 2), [PMIM][BF_4] (Figure 4), [BMIM][BF_4] (Figure 5), [AMIM][BF_4] (Figure 6), and also of [EMIM][PF_6] (Figure 7) are similar to the structures of the

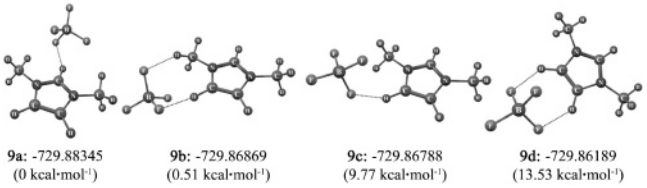

Figure 3. Stable [MMIM][BF_4] structures, their B3LYP/6-31G* (Hartree) electronic energies, and their energies relative to the global-minimum energy (in parenthesis). Short contacts between F and H atoms are indicated with dotted lines. **9a**, forward; **9b** and **9c**, methside; **9d**, back (see text for nomenclature).

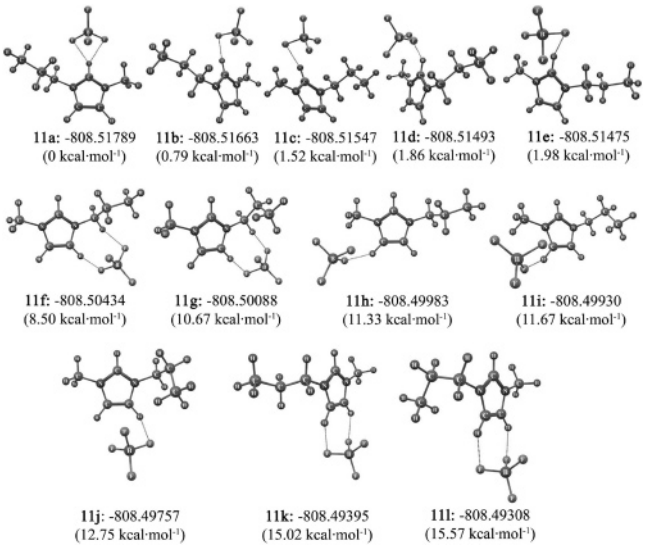

Figure 4. Stable [PMIM][BF_4] structures, their B3LYP/6-31G* (Hartree) electronic energies and their energies relative to the global-minimum energy (in parenthesis). Short contacts between F and H atoms are indicated with dotted lines. **11a**−**11e**, forward; **11f**−**11h**, ethside; **11i**, methside; **11j**−**11l**, back (see text for nomenclature).

EMIM halides with two exceptions: (i) the top minimum does not exist even in vacuum, and (ii) all the structures are nonplanar. The anion in the global minimum structure is positioned over the ring plane and has a short contact with H−C(2). When the H2 proton is substituted by a methyl group in [EDMIM][BF_4] (Figure 8), the BF_4^- anion in global minimum structure is shifted to a more upward position, which more closely resembles the top structure characteristic of the EMIM halides.

Following the descriptions of the "gross" positions of the anion, a number of subconfigurations can be described arising from variations in the conformation of alkyl groups. These latter positions are determined by the torsion angles: τ_1 = C2−N1−C6−C7, τ_2 = N1−C6−C7−C8, and τ_3 = C6−C7−C8−C9. When $\tau_1 \approx 90°$, the alkyl group adopts a nonplanar orientation relative to the plane of the imidazolium ring, whereas $\tau_1 \approx 0°$ describes another less stable conformation with the N1−C6−C7 moiety lying in the plane of the ring, but this minimum

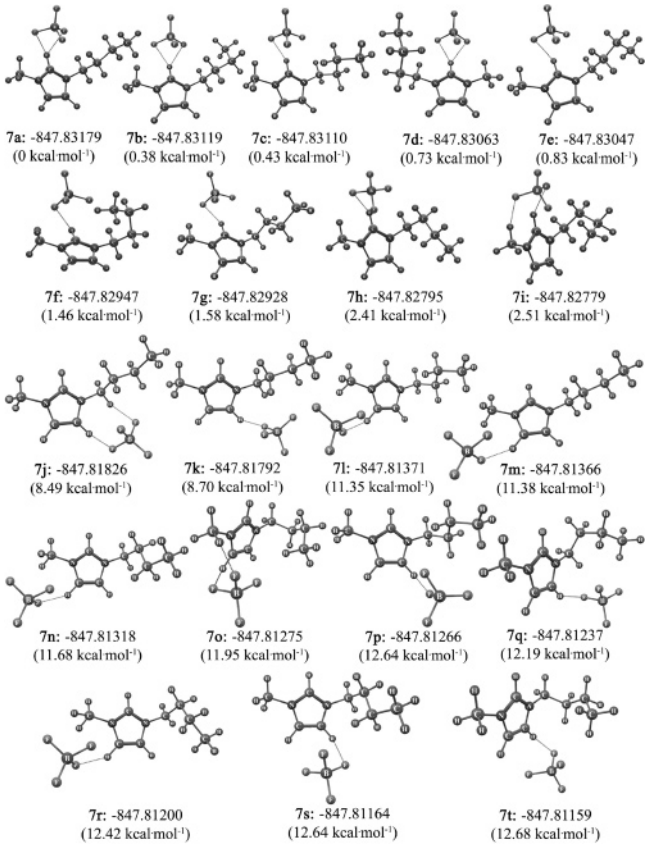

Figure 5. Some stable [BMIM][BF_4] structures, their B3LYP/6-31G* (Hartree) electronic energies, and their energies relative to the global-minimum energy (in parenthesis). Short contacts between F and H atoms are indicated with dotted lines. **7a**−**7i**, forward; **7j**−**7k**, **7p**, and **7q**, butside; **7l**−**7o**, methside; **7s** and **7t**, back (see text for nomenclature).

disappears when the $AlkMIM^+-BF_4^-$ forward structures are optimized. This "in-plane-of-the-ring" conformation corresponds to local minima for side structures, e.g., **1j** and **1k** in Figure 2. It was not possible to find any minima with $\tau_1 \approx 180°$. For τ_2 and τ_3 in stable staggered conformations, the usual values of ca. 180° and ca. 60° are adopted.

Overall, potential energy surfaces of **6**, **7**, and **9**−**13** have from five to more than twenty local minima found by geometry optimization (Figures 2−8). In all cases, forward structures are energetically more stable by ca. 7−17 kcal/mol than all other structures. To evaluate the possible effect of the surrounding medium on the relative energy of the minima, we simulated a solution of **6** in CH_2Cl_2 within the PCM framework.[49] According to these computations, the energy gaps between the forward structure and all other structures are smaller in CH_2Cl_2 than in vacuum (Figure 2) but still about twice or even three times as large as that of **2** in CH_2Cl_2. These more pronounced energy differences result in a low population of back and/or side minima in comparison with global forward minimum, as will be discussed later. It also is worth mentioning here that the BF_4^- anion in the forward structure in CH_2Cl_2 is situated closer to the plane of the imidazolium ring than in the corresponding vacuum structure **2a**.

Vibrational Spectra, Mode of Binding, and Conformations of the ILs. The IR and Raman spectra of the ionic liquids **6**, **7**, and **9**−**13** and of the CD_2Cl_2 solutions of **6**, **7**, [EDMIM][BF_4] (**10**), and [PMIM][BF_4] (**11**) obtained at 25° C are shown in Figures 9−15, and the band positions are listed in Tables 1−6 (and Supporting Information, Tables 2S, 3S) together with assignments based on comparison of the spectra of all the studied

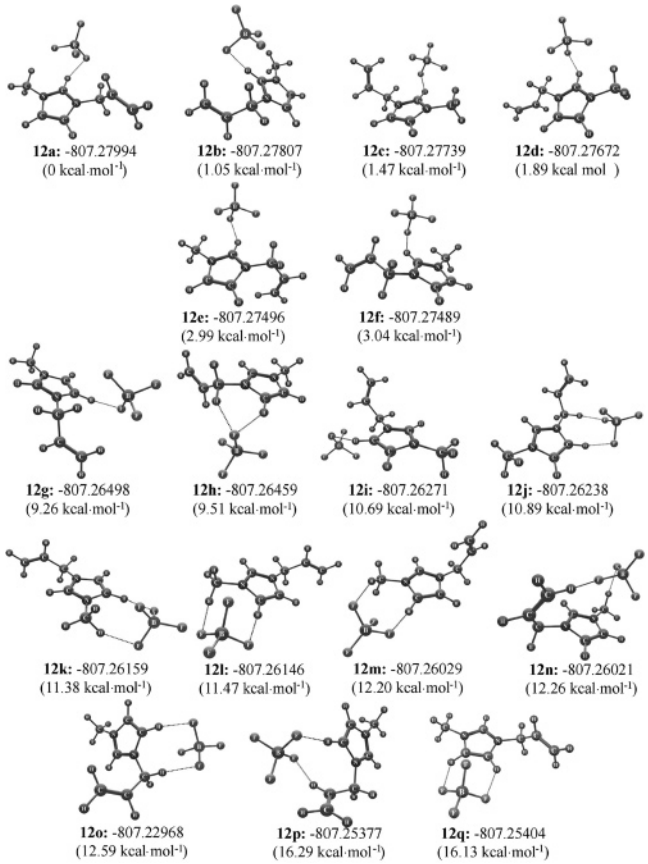

Figure 6. Stable [AMIM][BF_4] structures, their B3LYP/6-31G* (Hartree) electronic energies, and their energies relative to the global-minimum energy (in parenthesis). Short contacts between F and H atoms are indicated with dotted lines. **12a**−**12f**, forward; **12g**−**12j**, **12o**, and **12p**, allside; **12k**−**12m**, methside; **12n**, top; **12q**, back (see text for nomenclature).

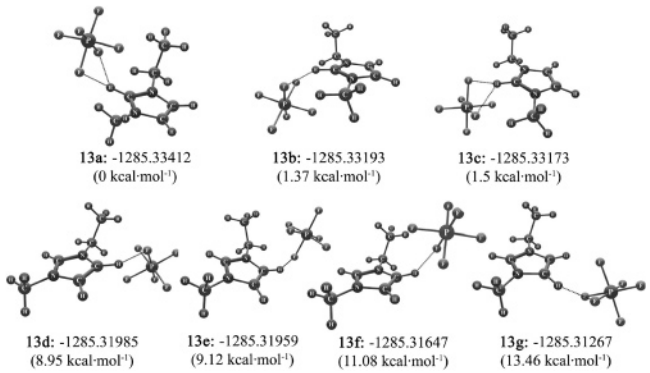

Figure 7. Stable [EMIM][PF_6] structures, their B3LYP/6-31G* (Hartree) electronic energies, and their energies relative to the global-minimum energy (in parenthesis). Short contacts between F and H atoms are indicated with dotted lines. **13a**−**13c**, forward; **13d**−**13f**, ethside; **13g**, methside (see text for nomenclature).

compounds and on the present SQM computations. The latter demonstrate a good general agreement between the calculated and the experimental wavenumbers of the fundamentals.

The data presented in Tables 1−6 (and Supporting Information, Tables 2S, 3S) show that the spectra of **6**, **7**, and **9**−**13** may be qualitatively analyzed in terms of the vibrational modes of the cation and those of the anion, because these modes practically do not mix and retain their individuality. Consequently, it is possible to compare the vibrational frequencies of the separated ions (see Supporting Information, Tables 4S−6S) with the ion pairs (Tables 1−6 and Supporting

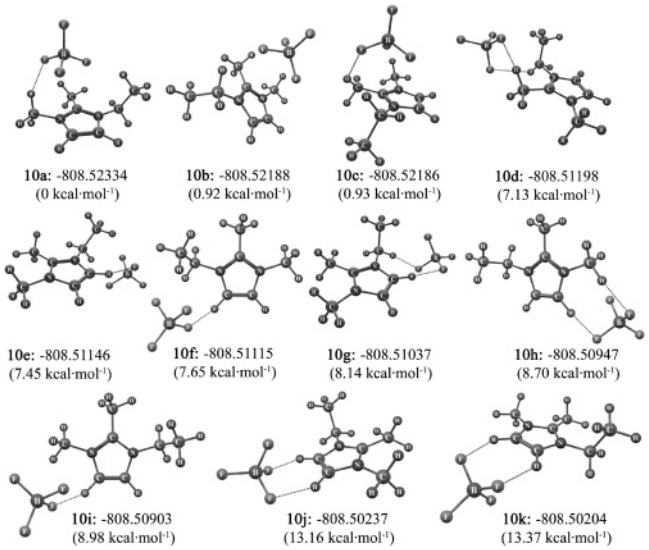

Figure 8. Stable [EDMIM][BF_4] structures, their B3LYP/6-31G* (Hartree) electronic energies, and their energies relative to the global-minimum energy (in parenthesis). Short contacts between F and H atoms are indicated with dotted lines.

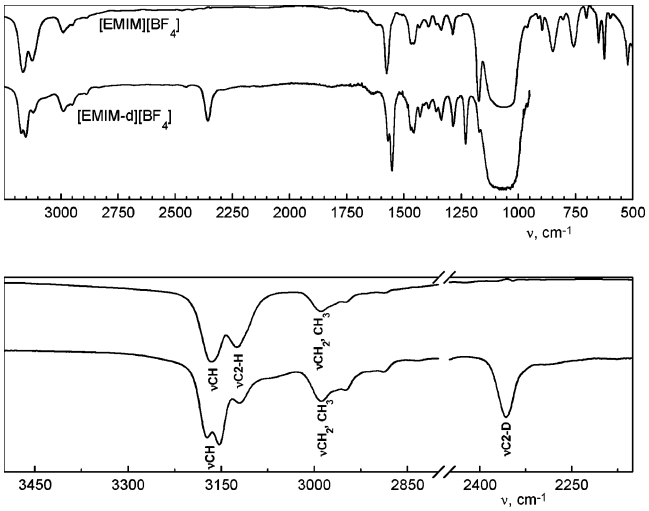

Figure 9. IR spectra of [EMIM][BF_4] and [EMIM-d][BF_4] in which the D-atom is in the 2-position of the ring.

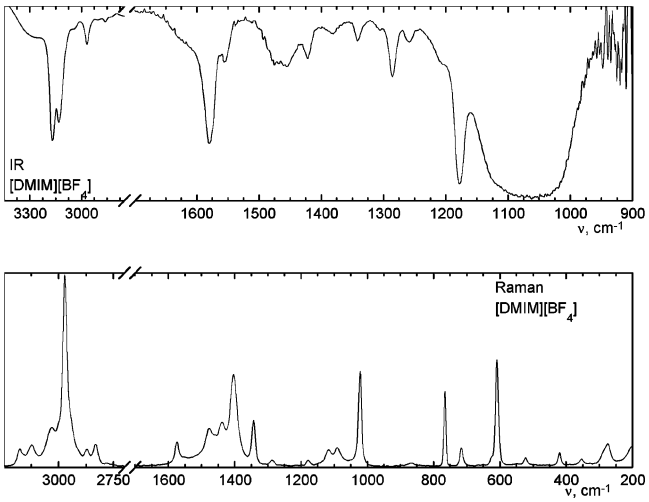

Figure 10. Vibrational spectra of [DMIM][BF_4].

Information, Tables 2S, 3S). Our computations demonstrate that the ion pair formation strongly influences BF and PF stretching vibrations of the BF_4^- and the PF_6^- anion, respectively and

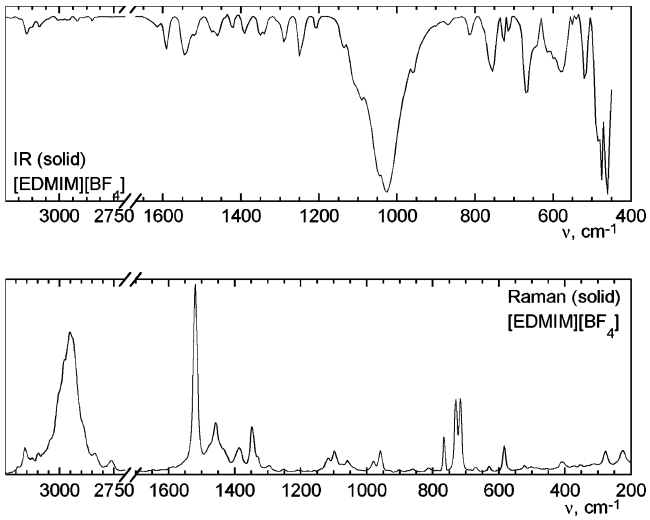

Figure 11. Vibrational spectra of [EDMIM][BF_4].

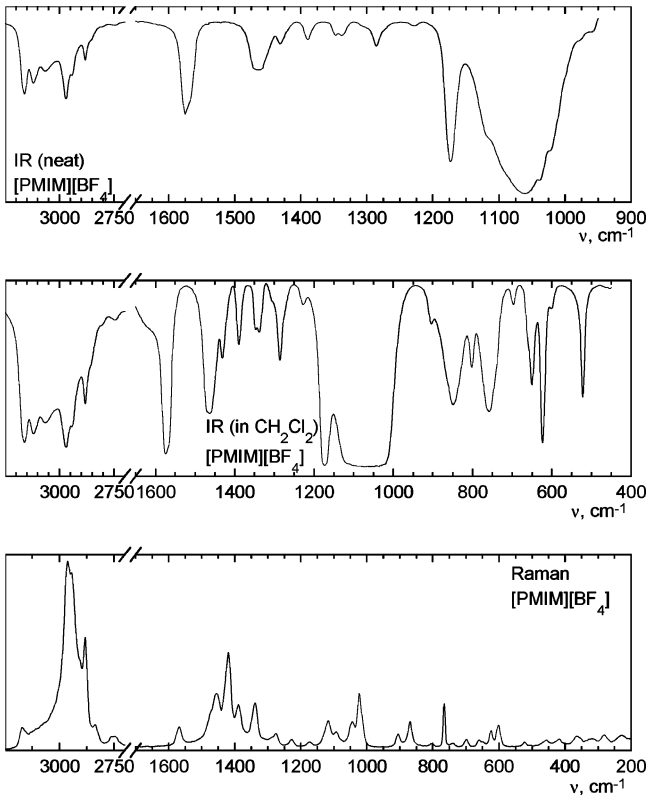

Figure 12. Vibrational spectra of [PMIM][BF_4].

out-of-plane and stretching vibrations of the C2−H, C4−H and C5−H bonds of the cation (Tables 1−6). Some out-of-plane vibrations of the imidazolium ring also are changed in comparison with the isolated cation. All other fundamentals are almost completely transferable between the individual ions and the corresponding ion pair.

It is apparent that all three CH stretching modes of the imidazolium ring are practically degenerate in the absence of the anion, and as a result only the νCH band (ca. 3170 cm^{-1}) should be observed in the IR spectra for the isolated cation (Supporting Information, Table 4S). The red shift of one of these three overlapping bands (i.e., the νC2−H band of **6a** in Table 1), caused by the interaction with the anion, removes the degeneracy, and the second band at ca. 3130 cm^{-1} arises in the spectra of liquids **6**, **7**, **9**, and **11**−**13**. By analogy with the "haloid interaction bands",[6−8] this lower frequency band may

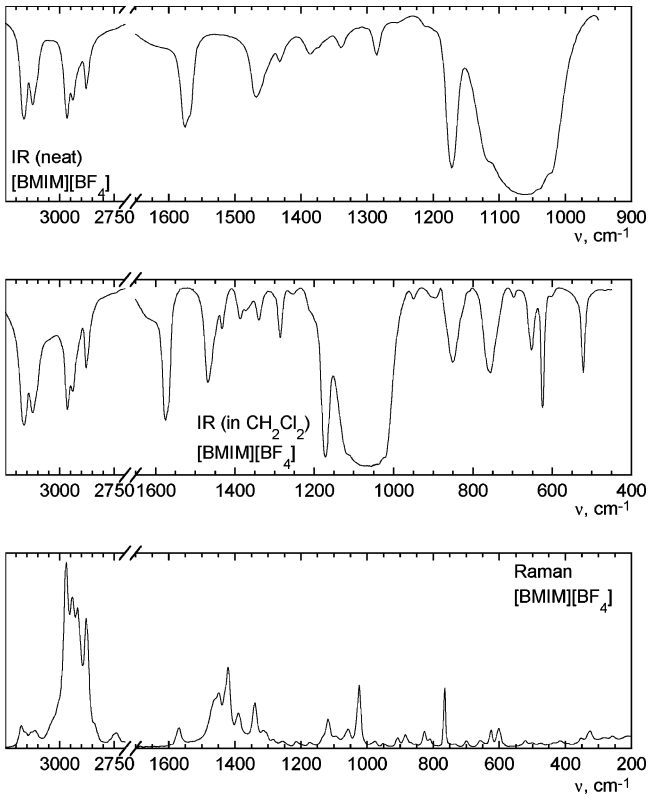

Figure 13. Vibrational spectra of $[BMIM][BF_4]$.

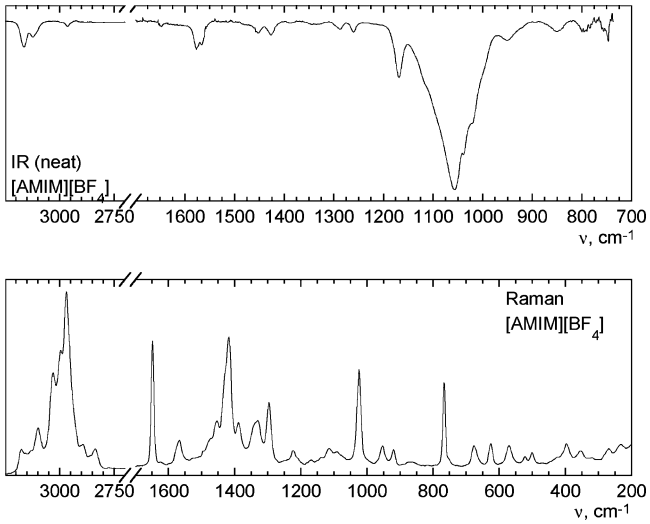

Figure 14. Vibrational spectra of $[AMIM][BF_4]$.

be ascribed to hydrogen bonding between the cation and the anion. According to computations, the short contact of H2 with the anion induces not only a red shift of the νC(2)−H band, but also a substantial growth of its IR intensity (Table 1, **6a**). The latter is regarded as the most reliable marker of H-bond formation,[50] though this effect is overestimated by B3LYP computations. Furthermore, the dramatic increase of the C(2)−H out-of-plane frequency of the cations during the course of ion pair formation (cf. Tables 1 and Supporting Information, 4S) is strongly indicative of hydrogen bonding.

It should be mentioned that reliable assignment of the out-of-plane vibrations of the imidazolium C−H moieties (γCH) is complicated by the fact that their blue shifts and the growth of intensity of the corresponding IR bands, caused by the ion pair formation, are overestimated by B3LYP/6-31G* computations, e.g., the frequency of γC2−H for **6a** is about 985 cm^{-1} (see Table 1). The use of a larger basis set by Heimer et al.[32] resulted in the prediction of a lower γC2−H frequency of 944 cm^{-1}. We have tried to evaluate this frequency within the framework of BPW91/cc-pVTZ computations, which usually reliably yields vibrational parameters of molecules even without scaling,[51] and obtained a wavenumber of 911 cm^{-1} for γC2−H bonded to the BF_4^- anion. Calculated frequencies of γC−H vibrations for two other imidazolium CH groups, free from the bonding to the anion, are about 810 and 720 cm^{-1} irrespective of the DFT functional and basis set used. Experimental IR spectra of the ILs studied usually contain several weak bands in the region around 900 cm^{-1} and one band of medium intensity at about 850 cm^{-1}. A weak but reliably detectable line at ca. 860 cm^{-1} is observed in the Raman spectra of the compounds under study. Most likely, one of these spectral features should be assigned to the out-of-plane vibrations of the CH group bonded to the anion, while the IR and Raman bands around 700 and 800 cm^{-1} belong to in-phase and out-of-phase γC−H vibrations, respectively, of the remaining two nonbonded imidazolium CH groups.

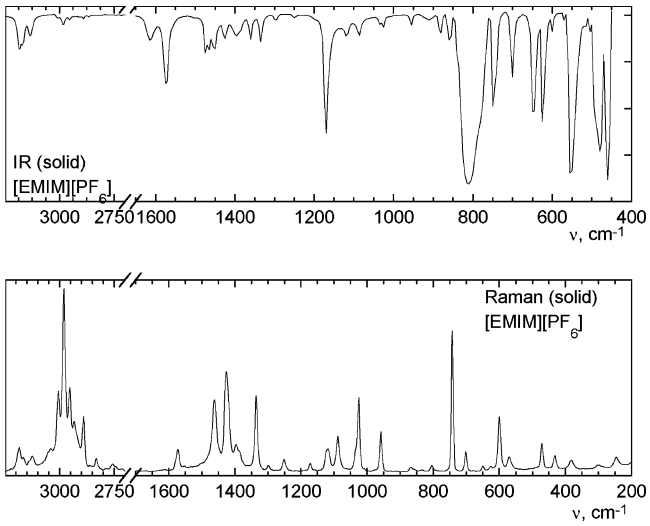

Figure 15. Vibrational spectra of $[EMIM][PF_6]$.

Our DFT computations, both B3LYP/6-31G* and BPW91/cc-pVTZ, seem to overestimate not only the blue shift of γC−H but also the red shift of νC−H for back or side structures (e.g., νC4−H or νC5−H for **6h** and **6j**, respectively, in Table 1). Both Raman and IR spectra of the ILs contain the νCH band (ca. 3170 cm^{-1}), which belongs to in-phase and out-of-phase νC−H vibrations of two nonbonded imidazolium CH groups. Another IR and Raman feature at ca. 3110−3130 cm^{-1} should be assigned to the stretching vibrations of the CH group bonded to the anion. From the comparison of these experimental bands with the DFT predictions (see Table 1), it is not clear whether the computations incorrectly predict the wavenumbers for νC4−H and νC5−H for **6h** and **6j**, respectively, or whether the structures **6h** and **6j** do not exist in detectable concentrations under the experimental conditions. To clarify this important issue, we recorded the IR spectrum of partially deuterated (C2−D) $[EMIM][BF_4]$ (Figure 9). The comparison of the spectra of $[EMIM][BF_4]$ and $[EMIM\text{-}d][BF_4]$ demonstrates that the position of the νCH band at ca. 3170 cm^{-1} remains essentially unchanged after deuteration, but it becomes a doublet. The second band at ca. 3130 cm^{-1} almost disappears in the spectrum of $[EMIM\text{-}d][BF_4]$, while a new strong band appears at 2358 cm^{-1}. Thus, the band at ca. 3130 cm^{-1} belongs mainly to the stretching vibrations of C2−H group H-bonded to the anion,

TABLE 2: Vibrational Spectra of [EMIM-d][BF_4]

	computations [ν,[b] cm^{-1} (I_{IR}, km/mole; I_{Ra}, $Å^4$/AMU)]			assignnment[c]
IR ν/cm^{-1}, I[a]	**6a**	**6h**	**6j**	
3174 m	3178 (1; 100)	3170 (0; 95)		νC4−H,C5−H (in-phase)
3156 m	3161 (4; 51)		3169 (5; 75)	νC4−H,C5−H (out-of-phase)
3121 w				
		2999 (454; 110)		ν C4−H
			2978 (507; 165)	ν C5−H
2989 m−w	3007 (14; 41)	3022 (11; 69)	3042 (4; 53)	ν_{as} CH_3 (Me)
	2995 (0; 14)	3018 (107; 81)	3010 (27; 43)	ν_{as} CH_3, CH_2
2967 w sh	2984 (1; 54)	2972 (16; 5)	2992 (5; 82)	ν_{as} CH_3, CH_2
	2982 (9; 75)	2964 (22; 107)	2964(19; 105)	ν_{as} CH_3 (Me)
2948 w	2949 (22; 96)	2950 (0; 91)	2948 (7; 75)	ν_{as} CH_3 (Et)
			2931 (30; 62)	ν_s CH_2
2911 vvw	2913 (32; 117)	2914 (16; 82)	2916 (24; 160)	ν_s CH_2
2886 vw	2905 (36; 152)	2910 (49; 148)		ν_s CH_3 (Me)
	2885 (26; 109)	2892 (9; 122)	2874 (22; 111)	ν_s CH_3 (Et)
2358 s	2345 (244; 46)	2356 (13; 17)	2369 (9; 45)	ν C2−D
1569 s	1577 (17; 4)	1589 (55; 1)	1585 (50; 1)	ν C═C
1552 vs	1550 (51; 2)	1550 (35; 2)	1559 (38; 2)	ν_{as} N1C2N3, r C2−D
1548 sh				
1543 sh				
1470 m	1475 (5; 7)	1468 (47; 15)	1490 (2; 19)	δ_{as} CH_3 (Et)
	1465 (8; 21)	1466 (15; 9)	1471 (6; 10)	δ_{as} CH_3 (Me)
1457 m	1461 (12; 15)	1460 (13; 21)	1468 (9; 18)	δ_{as} CH_3 (Me)
	1458 (11; 9)	1446 (6; 23)	1457 (22; 24)	δ CH_2
	1448 (2; 29)	1445 (4; 14)	1447 (11; 18)	δ_{as} CH_3 (Et)
1430 w	1428 (11; 16)	1430 (13; 14)	1436 (5; 12)	δ_s CH_3
1411 vvw	1414 (4; 28)	1405 (6; 13)	1416 (30; 15)	δ CH_2, ν ring
1390 m	1393 (12; 3)	1390 (5; 4)	1386 (9; 13)	δ_s CH_3 (Et), w CH_2
	1375 (2; 9)	1366 (8; 20)	1382 (12; 4)	ν_{as} C2N1C5, δ_s CH_3(Et)
1358 m	1358 (7; 1)	1360 (8; 20)	1332(19; 24)	w CH_2
1335 m	1315 (10; 24)	1317 (24; 34)	1311 (27; 15)	ν N−Et, N−Me, breathing
	1283 (2; 2)	1293 (2; 5)	1298 (4; 8)	r C4−H, C5−H, t CH_2
1285 m	1256 (473; 0)	1231(471; 0)	1234(523; 1)	ν BF_4
1250 vw		1250 (2; 5)	1241 (19; 7)	r C2−D, rC4−H, νN−Et, νN−Me
1229 s	1222 (8; 3)			r C2−D, rC4-H, νN−Et, νN−Me

[a] Labels: w, weak; m, medium; s, strong; v, very; sh, shoulder; br, broad. [b]SQM scaled wavenumbers. [c]Labels: ν, stretch; δ, bend; w, wagging; t, twisting; r, rocking; γ, out-of-plane; s, symmetrical; as, antisymmetrical.

while the band at ca. 3170 cm^{-1} should be assigned to the stretching vibrations of the C4−H and C5−H groups free from H-bonding. It is likely that the weak band at 3121 cm^{-1} in the spectrum of [EMIM-d][BF_4] belongs to the stretching vibrations of C4−H and/or C5−H groups H-bonded to the anion. The low intensity of this band can be explained by the low concentration of the structures **6h** and/or **6j** in the liquid state. This explanation agrees well with computationally predicted higher energetic stability of **6a** in comparison with **6h** and **6j** and with all other back- or side-forms (see Figure 2). Nevertheless, during low-temperature crystallization of **6,** the dominant form in the liquid state, viz. **6a**, is not observed but instead the compound crystallizes with the structure **6h**.[38] The presence of both the forward- and back- and/or side-forms in the [EMIM][BF_4] liquid is further confirmed by two-dimensional NMR spectroscopic data;[52] HOESY results reveal that the anion does not occupy a specific position in this salt. Moreover, in CH_2Cl_2 in which the PGSE data show almost complete ion pairing, there are strong, nonselective NOE contacts between the cation and anion that eliminates hydrogen bonding as the primary source of the interaction between the cation and anion. However, from these NMR data, it was not evident that the major form of [EMIM][BF_4] in the liquid is **6a**.

The spectra of all the other ILs studied, including [EMIM][PF_6], in the region of 3100−3200 cm^{-1} essentially coincide with the spectra of **6** discussed above. This most likely implies that in all these imidazolium salts, the large and weakly coordinating perfluoro anions are mainly situated near the H(C2) proton. Hydrogen bonding with this acidic proton may be one of the reasons why this position is favored, although the small shift of νC(2)−H indicates that the H-bond is weak and could be easily destroyed by dissolving the compound in a molecular (organic) solvent. Nevertheless, the spectra of **6** in the CD_2Cl_2 solution remains essentially unchanged in the νCH region, except that the νC(2)-H band becomes a doublet. The spectra do not exhibit any other spectral markers of isolated cations or anions (Tables 4S−6S), that is, ion pairing is not destroyed by the solvent. It is therefore reasonable to assume that the $EMIM^+$ and BF_4^- ions are held together mainly by strong Coulomb attractions, and that H-bonding plays only a minor role. The latter is clear from the computed energy of the ion pair formation in CH_2Cl_2, which equals 14 kcal/mol at the B3LYP/6-31G* level (within the framework of PCM[49]).

As already mentioned, both the imidazolium CH vibrations and the stretching vibrations of the anions are influenced by ion pair formation. In contrast to the CH modes discussed above, however, the assignment for the BF_4^- and PF_6^- vibrations is straightforward, even on the basis of a comparison of the vibrational spectra of the ILs with some published spectra of other compounds, e.g., $NaPF_6$.[53] The remaining parts of the spectra, including vibrations of alkyl groups and of imidazolium ring (except νCH and γCH), do not depend on the interactions between the ions but on the conformation of the cation.

In the case of [EMIM][BF_4], the calculated spectra of the

TABLE 3: Vibrational Spectra of [EMIM][PF_6]

experiment (ν/cm^{-1}, I^a)		computations [ν, cm^{-1b} (I_{IR}, km/mole; I_{Ra}, Å^4/AMU)]			assignment^c
IR (KBr)	Raman	**13b**	**13f**	**13g**	
3183 m	3184 m	3178^d (0; 115/ 0.13)	3188 (17; 75/ 0.18)	3193 (54; 68/ 0.19)	ν C4−H,C5−H (in-phase)
3168 m	3165 m	3161^e (9; 40/ 0.74)	3171 (11; 43/ 0.29)	3170 (13; 48/ 0.28)	ν C4−H,C5−H (out-of-phase)
3133 m	3138 sh	3160^f (234; 55/ 0.28)			ν C2−H
	3125 m		3147 (182; 68/ 0.32)		ν C5−H
				3094 (265; 105/ 0.27)	ν C4−H
3007 m	3005 s	3022 (6; 38/ 0.74)	3003 (5; 32/ 0.67)	3001 (5; 56/ 0.74)	ν_{as} CH_3 (Me)
2981 m	2979 vs	2988 (6; 71/ 0.74)	2999 (4; 53/ 0.74)	2991 (2; 69/ 0.75)	ν_{as} CH_3, CH_2
2982 m		2988 (7; 11/ 0.71)	2984 (3; 75/ 0.75)	2974 (15; 6/ 0.74)	ν_{as} CH_3, CH_2
2954 m	2953 s	2970 (2; 67/ 0.66)	2965 (20; 65/ 0.61)	2965 (15; 99/ 0.58)	ν_{as} CH_3 (Me)
2930 vw	2932 m	2958 (14; 99/ 0.65)	2951 (9; 89/ 0.75)	2952 (1; 90/ 0.75)	ν_{as} CH_3 (Et)
2924 vw		2921 (14; 82/ 0.11)	2911 (16; 162/ 0.02)	2916 (13; 83/ 0.09)	ν_s CH_2
2912 vw	2915 sh	2913 (24; 148/ 0.05)	2910 (22; 77/ 0.13)	2914 (12; 128/ 0.02)	ν_s CH_3 (Me)
2904 vw		2894 (14; 122/ 0.04)	2896 (19; 127/ 0.06)	2893 (8; 118/ 0.02)	ν_s CH_3 (Et)
2889 w	2889 m				
1613 m	1611 vw				
1572 s	1572 m	1584 (27; 3/ 0.40)	1602 (26; 4/ 0.49)	1581 (69; 5/ 0.46)	ν C═C
		1573 (39; 3/ 0.48)	1579 (75; 0.62/ 0.72)	1564 (64; 4/ 0.6)	ν_{as} N1C2N3, r C2H
1473 m		1470 (7; 10/ 0.74)	1493 (5; 14/ 0.75)	1467 (3; 17/ 0.75)	δ_{as} CH_3 (Et)
		1468 (7; 19/ 0.74)	1486 (8; 11/ 0.73)	1464 (8; 4/ 0.56)	δ_{as} CH_3 (Me)
1466 m	1461 s	1456 (13; 13/ 0.75)	1484 (20; 14/ 0.73)		δ_{as} CH_3 (Me)
		1448 (16; 16/ 0.75)	1448 (5; 24/ 0.74)	1448 (17; 20/ 0.75)	δ CH_2
1452 m	1451 sh	1445 (3; 26/ 0.60)	1437 (11; 18/ 0.75)	1445 (5; 24/ 0.74)	δ_{as} CH_3 (Et)
1426 m	1426 s	1429 (4; 12/ 0.75)	1425 (14; 16/ 0.65)	1435 (11; 18/ 0.75)	δ_s CH_3
1421 sh	1420 sh	1421 (7; 28/ 0.24)	1414 (6; 4/ 0.53)	1424 (15; 15/ 0.71)	δ CH_2, ν ring
1402 sh			1405 (1; 10/ 0.34)	1408 (6; 10/ 0.35)	ν_{as}C2N1C5, $\delta_s$$CH_3$ (Et)
1395 m	1396 w	1393 (9; 8/ 0.34)		1391 (5; 7/ 0.31)	δ_s CH_3 (Et), w CH_2
1384 sh	1386 sh	1375 (2; 4/ 0.12)	1384 (15; 28/ 0.14)	1375 (21; 21/ 0.19)	ν_{as}C2N1C5, ν_{as} C2N3C4, $\delta_s$$CH_3$ (Et)
1360 m		1356 (26; 7/ 0.60)	1367 (17; 2/ 0.71)	1363 (20; 2/ 0.71)	w CH_2
1335 m	1335 s	1322 (8; 17/ 0.25)	1326 (9; 27/ 0.42)	1323 (13; 24/ 0.42)	ν N−Et, N−Me, breathing
1300 w					
1295 w	1300 w	1293 (0; 3/ 0.62)	1297 (3; 1/ 0.75)	1283 (0; 2/ 0.66)	r C4−H, C5−H, t CH_2
1250 w	1250 w	1258 (15; 3/ 0.65)	1255 (1; 5/ 0.61)	1249 (2; 6/ 0.62)	r C2−H
1198 sh					
1170 vvs	1172 m	1161 (109; 2/ 0.69)	1170 (104; 2/ 0.52)	1164 (76; 2/ 0.74)	ν N−Et, N−Me
1133 sh	1123 m	1139 (0; 3/)0.73	1131 (0; 2/ 0.72)	1131 (0; 2/ 0.69)	r CH_3
1118 m	1117 m	1129 (18; 2/ 0.65)	1124 (3; 3/ 0.36)	1119 (18; 6/ 0.23)	r CH_2, r CH_3 (Et)
		1103 (0; 2/ 0.42)	1088 (6; 4/ 0.21)	1082 (6; 7/ 0.11)	r CH_3
1094 sh		1097 (2; 7/ 0.20)	1119 (12; 2/ 0.34)	1109 (44; 7/ 0.53)	r C−H
1087 m	1088 m	1089 (12; 6/ 0.46)	1077 (3; 5/ 0.29)	1080 (2; 2/ 0.62)	r CH_3
1034 w	1034 sh	1029 (7; 7/ 0.38)	1027 (1; 3/ 0.43)	1024 (0; 8/ 0.27)	δ ring
1026 w	1025 s	1021 (2; 6/ 0.19)	1014 (1; 8/ 0.11)	1010 (2; 6/ 0.12)	breathing, νN−Et, νN−Me
955 w	958 m	941 (38; 1/ 0.56)			ν CC (Et)
911 w br	912 vw	949^g (5; 4/ 0.19)			γ C2−H
			933 (29; 0/ 0.59)	938 (74; 1/ 0.74)	γ C4−H, γ C5−H
				908 (1; 6/ 0.35)	ν C−C (Et)
			886 (363; 0/ 0.69)		γ C4−H, γ C5−H
882 m		937 (355; 0/ 0.71)	936 (1; 7/ 0.32)	939 (459; 0/ 0.69)	ν PF_6
858 m	868 vw		931 (393; 0/ 0.74)		ν PF_6
839 sh	852 vw	917 (256; 0/ 0.73)	923 (327; 0/ 0.74)	923 (392; 1/ 0.64)	ν PF_6
810 vvs	803 w	903 (471; 0/ 0.74)		913 (322; 0/ 0.66)	ν PF_6, γ C2−H
		813 (0; 0/ 0.35)			γ CH
780 s sh		795 (16; 0/ 0.36)	794 (6; 0/ 0.60)	799 (15; 0/ 0.75)	r CH_2, r CH_3 (Et)
			782 (82; 0/ 0.75)	787 (3; 0/ 0.61)	r CH_2, r CH_3 (Et)
748 s	742 s	705 (42; 11/ 0.02)	724 (35; 10/ 0.02)	727 (29; 9/ 0.08)	ν_s PF_6
742 sh					
		721 (25; 2/ 0.75)			γ C4−H, C5−H
		720 (13; 2/ 0.75)			ν N−Me, ν N−Et
701 s	701 m		713 (8; 3/ 0.63)	708 (7; 4/ 0.16)	γ C2−H, ν N−Me, ν N−Et
			695 (9; 0/ 0.62)	698 (3; 0/ 0.70)	γ C2−H, γ C4−H, γ C5−H,
647 vs	649 vw	657 (42; 1/ 0.37)	654 (18; 0/ 0.56)	648 (12; 0/ 0.35)	γ N−Et, γ C2−H
637 sh					
623 s	625 vw	620 (4; 1/ 0.60)	621 (6; 1/ 0.69)	621 (5; 0/ 0.70)	γ N−Me, ring-packering
600 m	599 m	589 (1; 5/ 0.30)	591 (2; 6/ 0.2)	589 (1; 5/ 0.2)	δ N1−C2-N3
590 w					
583 w		586 (12; 1/ 0.55)	596 (7; 1/ 0.74)	598 (5; 1/ 0.58)	ν PF_6
577 w					
570 w	569 m	570 (19; 1/ 0.74)	572 (17; 1/0.5)	583 (10; 1/ 0.74)	ν PF_6
552 vvs	558 sh	547 (56; 0/ 0.48)	545 (54; 0/ 0.17)	550 (54; 0/ 0.37)	δ PF_6
543 sh	546 vw	544 (20; 0/ 0.50)	545 (22; 0/ 0.31)	545 (25; 0/ 0.4)	δ PF_6
528 sh	535 vvw	542 (24; 0/ 0.75)	543 (28; 0/ 0.66)	545 (25; 0/ 0.51)	δ PF_6
522 m					
512 m					
504 m					

TABLE 3: Continued

experiment (ν/cm^{-1}, I^a)		computations [ν, cm^{-1b} (I_{IR}, km/mole; I_{Ra}, Å^4/AMU)]			assignment^c
IR (KBr)	Raman	**13b**	**13f**	**13g**	
491 s					
481 vvs	478 sh	463 (3; 2/ 0.74)	463 (3; 2/ 0.75)	465 (3; 2/ 0.71)	δ PF_6
475 vvs	471 m	457 (0; 0/ 0.52)	455 (1; 1/ 0.75)	459 (0; 1/ 0.72)	δ PF_6
466 s		451 (0; 1/ 0.62)	450 (0; 1/ 0.75)	450 (0; 1/ 0.69)	δ PF_6
458 vvs					
	430 m	435 (0; 1/ 0.55)	429 (1; 1/ 0.25)	433 (1; 1/ 0.3)	r N−Et, r N−Me
	381 m	377 (4; 1/ 0.15)	381 (2; 1/ 0.48)	377 (0; 1/ 0.2)	δ NEt (NCC)
	300 w	309 (1; 1/ 0.75)	309 (1; 0/ 0.75)	312 (0; 0/ 0.22)	tors CH_3 (Et)
		307 (0; 0/ 0.75)	302 (0; 0/ 0.73)	303 (1; 0/ 0.71)	δ PF_6
		301 (0; 0/ 0.62)	296 (0; 0/ 0.75)	295 (0; 0/ 0.66)	δ PF_6
		293 (0; 0/ 0.65)	295 (0; 0/ 0.69)	294 (0; 0/ 0.64)	δ PF_6
	246 m	244 (2; 2/ 0.7)	236 (6; 2/ 0.71)	229 (2; 1/ 0.70)	γ N−Me, ring-packering
		226 (1; 0/ 0.7)	227 (2; 0/ 0.56)	208 (1; 0/ 0.75)	torsEt

[a] Labels: w, weak; m, medium; s, strong; v, very; sh, shoulder; br, broad. [b]SQM scaled wavenumbers. [c]Labels: ν, stretch; δ, bend; w, wagging; t, twisting; r, rocking; γ, out-of-plane; s, symmetrical; as, antisymmetrical. [d]This frequency computed with BPW91/cc-pVTZ is equal to 3236 cm^{-1} (without scaling). [e]This frequency computed with BPW91/cc-pVTZ is equal to 3217 cm^{-1} (without scaling). [f]This frequency computed with BPW91/cc-pVTZ is equal to 3155 cm^{-1} (without scaling). [g]This frequency computed with BPW91/cc-pVTZ is equal to 904 cm^{-1} (without scaling).

in-plane-of-the-ring (**6j** in Table 1) and out-of-plane-of-the-ring (**6a** in Table 1) conformations of the ethyl moiety differ strongly in two regions: (i) 600−650 cm^{-1} (puckering of the imidazolium ring, mixed with out-of-plane vibrations of the N−Me and N−Et moieties); (ii) 350−400 cm^{-1} (in-plane bending of the N−Et group). The absence of any "extra" bands in these regions suggests that the most energetically stable conformer **6a** dominates in the liquid state and the concentration of the conformer **6j** is too low to be detected in the IR or Raman spectra. Umebayashi et al.[26] ascribed the complicated shape of the Raman line at 438 cm^{-1} to a conformational equilibrium of the in-plane-of-the-ring and out-of-plane-of-the-ring forms of the [EMIM] cation, because the planar conformer showed only one vibration in this region. However, the doublet Raman line at 438 cm^{-1} also can be explained by an equilibrium between **6a** and **6h** (see Table 1). Consequently, it is not improbable that in addition to the sructure **6a** that dominates in the liquid state, some other forms of [EMIM][BF_4] exist, but on the basis of present computational and spectroscopic data it is not possible to determine unequivocally these minor forms.

In the case of **7**, **10**, **11**, and [EMIM][PF_6] (**13**), it was not possible to find a minimum on the potential energy surface corresponding to the in-plane-of-the-ring conformation of the 1-alkyl moiety. Therefore, only one conformation was regarded for **10** (Table 2S) and **13** (Table 3). Calculated spectra of *gauche*- (**11c)** and *anti*- (**11a)** conformers of [PMIM][BF_4] are listed in Table 4. According to computations, the vibrational frequencies of **11c** and **11a** differ essentially in the regions 1220−1270 cm^{-1}, 690−750 cm^{-1}, 370−460 cm^{-1}, and 300−330 cm^{-1}. Because the theoretical spectrum of the conformer **11c** fits with the experimentally determined spectra much better than the computational predictions for the conformer **11a**, the absence of any extra bands in the above mentioned regions suggests that **11c** dominates in the liquid state with the concentration of the *anti*-conformer **11a** being too low to be detected in the IR or Raman spectra.

For the [BMIM] cation, nine conformations can be considered because the butyl group of [BMIM][BF_4] is able to adopt these conformations: *anti,anti*; *anti,gauche*; *anti,-gauche*; *gauche,-anti*; *gauche,gauche*; *gauche,-gauche, -gauche,anti*; *-gauche,-gauche,* and *-gauche,-gauche* conformations. Only *anti,anti*- and *gauche,anti*- conformations were discussed by Berg et al.,[25] while Heimer et al.[32] described *anti,gauche* and *gauche,anti* conformers. According to Table 5, our experimentally determined spectroscopic data do not contradict the presence of all three conformers, but the Raman lines 473 and 392 cm^{-1} cannot be assigned to them, and at least one additional conformer, *gauche,gauche,* most likely participates in the conformational equilibrium.

The spectra of [AMIM][BF_4] (**12**) are presented in Figure 14 and vibrations are listed in Table 6. According to calculations, the most pronounced differences should be expected in the spectra of the conformers **12c** and **12a**, especially in the regions 530−570 cm^{-1} and 300−370 cm^{-1}. The theoretical spectrum of the conformer **12a** fits with the experimental data more closely than the computational predictions for conformer **12c**. The absence of any extra bands in the above mentioned regions suggests that **12a** dominates in the liquid state.

In summary, (1) six stable [EMIM][halide] ion pair structures were located in vacuum, with front, top, bottom, ethside, methside, and back possible locations. The front, top, and bottom structures are the lowest in energy with the side and the back structures lying ∼10−20 kcal/mol higher in energy. The PCM-simulated local structure around the cation in the CH_2Cl_2 solution is significantly different, the top and the bottom structures are absent, and the energy gap between the front and all other structures is only about 1 kcal/mol. These results are in agreement with ab initio MD simulations and could even explain why all the calculated structures (except the top and bottom) are evident in the various crystal structure determinations.

(2) Possible locations of perfluorinated anions BF_4^- and PF_6^- are similar to the structures of the halides, except that the top and the bottom minima do not exist, even in vacuum. All the structures are nonplanar and the PCM predicted energy gaps between the forward and all other structures in CH_2Cl_2 are about 2−3 kcal/mol.

(3) According to computations, the anion of each ion pair forms a H-bond with the (C2)H proton (the front structure) or with the (C4)H or (C5)H protons (side structures). The manifestation of these hydrogen bonds is a red shift of the νC2−H, νC4−H, and νC5−H bands in the IR spectra of the EMIM halides and of the νC2−H band in the IR and Raman spectra of the tetrafluoroborate and hexafluorophosphate species. There is not significant spectroscopic evidence to suggest H-bonding between the anions and the (C4)H or (C5)H protons.

(4) In the gas phase, the imidazolium cations and the anions obtain significant stabilization from association, ∼100 kcal/mol for [EMIM][BF_4], although in CH_2Cl_2 solution they gain in energy ca. 14 kcal/mol only at the B3LYP/6-31G* level (within the framework of PCM[51]). However, even this latter value is

TABLE 4: Vibrational Spectra of [PMIM][BF_4]

experiment (ν/cm^{-1}, I^a)		computations [ν, cm^{-1b} (I_{IR}, km/mole; I_{Ra}, Å^4·/AMU)]		assignments^c
IR neat (in CD_2Cl_2)	Raman	**11c**	**11a**	
		3180 (1; 94)	3178 (0; 104)	ν C4−H, C5−H (in-phase)
3160 s (3160 vs)	3172 w	3162 (4; 50)	3160 (4; 52)	ν C4−H, C5−H (out-of-phase)
3118 s (3118 vs)	3133 vw	3134 (213; 45)	3152 (204; 36)	ν C2−H
	3108 vw			
3061 m (3061 m)				
		3018 (15; 36)	3003 (12; 40)	ν_{as} CH_3 (Me)
(2989 sh)		2990 (7; 72)	2992 (0; 29)	ν_{as} CH_2
2968 s (2968 vs)	2965 vvs	2967 (3; 43)	2981 (8; 78)	ν_{as} CH_3 (Me)
2956 sh (2956 sh)	2957 sh	2954 (10; 32)	2957 (6; 13)	ν_{as} CH_2
2941 s (2941 vs)	2942 vs	2949 (25; 81)	2953 (16; 73)	ν_{as} CH_3 (Pr)
(2923 sh)		2926 (28; 69)	2932 (21; 79)	ν_{as} CH_3 (Pr)
	2906 sh	2910 (33; 158)	2909 (33; 121)	ν_s CH_2
		2907 (31; 110)	2903 (35; 155)	ν_s CH_3 (Me)
2881 s (2881 s)	2881 s	2880 (20; 120)	2872 (33; 98)	ν_s CH_2
2855 sh (2855 sh)		2866 (26; 108)	2867 (31; 81)	ν_s CH_3 (Pr)
	2836 w			
(1627 sh)				
1574 s (1574 vs)	1568 m	1584 (19; 3)	1581 (17; 4)	ν C═C
1567 sh (1555 sh)		1567 (47; 2)	1570 (51; 2)	ν_{as} N1C2N3, r C2−H
1473 sh (1470 sh)	1473 sh	1471 (10; 10)	1472 (5; 3)	δ_{as} CH_3
1464 s (1464 m)	1456 m	1464 (6; 16)	1470 (10; 17)	δ_{as} CH_3 (Me)
1462 m (1462 m)		1462 (5; 6)	1461 (1; 15)	δ_{as} CH_3 (Me)
1457 m (1452 s)		1454 (16; 13)	1461 (13; 20)	δ_{as} CH_3
		1451 (2; 23)	1453 (1; 27)	δ CH_2
		1447 (10; 19)	1452 (7; 9)	δ CH_2
1448 sh				
1431 m (1431 m)	1420 s	1431 (12; 13)	1430 (11; 17)	δ_s CH_3 (Me)
1415 sh (1426 sh)		1420 (5; 29)	1419 (4; 33)	ν ring
1389 m (1389 m)		1395 (7; 6)	1394 (2; 4)	δ_s CH_3
1388 sh	1389 m	1382 (0; 11)	1387 (6; 3)	ν_{as}C2N1C5
		1375 (4; 5)	1375 (1; 8)	w CH_2
1349 m (1349 m)		1358 (14; 3)	1337 (2; 13)	w CH_2
1337 m (1337 m)	1338 m	1321 (10; 21)	1312 (3; 13)	ν_s N−Pr, N−Me, breathing
1305 vw sh (1305 w sh)	1315 w sh		1310 (10; 10)	t CH_2
		1286 (1; 8)		t CH_2
1286 m (1286 s)	1285 sh	1256 (415; 0)	1234 (461; 0)	ν BF_4
1268 sh (1272 sh)	1274 m	1282 (2; 3)	1279 (1; 3)	r C−H
			1257 (8; 1)	t CH_2, r C−H
1227 m (1228 w)	1227 w	1220 (73; 2)		t CH_2, r C−H
1173 vvs (1173 vvs)	1173 w	1157 (176; 1)	1152 (148; 3)	r C2−H, ν N−Pr, N−Me
		1143 (1; 3)	1142 (45; 3)	r CH_3 (Me)
1119 sh (1119 sh)	1116 m	1129 (3; 4)	1135 (10; 3)	r CH_2, r CH_3 (Pr)
		1109 (10; 4)	1110 (6; 2)	r CH_3
1091 sh (1091 sh)	1093 m	1091 (8; 6)	1100 (9; 5)	r C−H
		1085 (6; 2)	1089 (15; 7)	r CH_3 (Pr), ν C−C
1063 vvs (1063 vvs)		1082 (171; 0)	1067 (190; 0)	ν BF, ν C═C
1037 vvs (1037 vvs)	1043 m	1041 (12; 5)	1041 (28; 3)	δ ring, (δ CNC)
1022 s (1022 s)	1022 s	1022 (31; 5)	1016 (20; 10)	breathing, νN−Pr, νN−Me
1009 sh (1009 sh)	1011 m, sh	1010 (61; 6)	1006 (20; 5)	ν C−C
(999 sh)		998 (230; 1)	998 (152; 1)	ν BF_4
(970 sh)				
		945 (36; 1)	984 (110; 0)	γ C2−H
(902 m)	905 w	892 (2; 2)		r CH_3 (Pr), w CH_2
			879 (0; 1)	r CH_3 (Pr), t CH_2
(868 sh)	870 m	840 (2; 8)	884 (6; 6)	ν_s C−C−C
(847 s)		815 (0; 0)	813 (0; 0)	γ C4−H, C5−H
(801 s)	803 vw	796 (11; 1)	753 (14; 1)	r CH_2
(757 s)	765 m	758 (9; 3)	757 (8; 3)	ν_s BF_4
			730 (9; 1)	ν N−Me, ν N−Pr
(738 sh)	739 w	725 (33; 2)	721 (29; 2)	γ C4−H, C5−H
(696 m)	698 w	691 (7; 2)		ν N−Me, ν N−Pr
(660 sh)	660 w		672 (32; 1)	γ N−Me, γ N−Pr
(650 s)	650 sh	667 (27; 0)		γ N−Me, γ N−Pr
			637 (8; 3)	δ N1−C2−N3
(622 vs)	625 m	627 (4; 1)	618 (0; 3)	γ N−Pr, N−Me, ring-packering
(601 m)	600 m	589 (0; 5)		δ N1−C2−N3
		526 (21; 1)	525 (20; 1)	δ BF_4
(521 s)	521 w	517 (3; 0)	514 (3; 0)	δ BF_4
		510 (2; 0)	511 (1; 0)	δ BF_4
	456 w	443 (1; 1)		δ N1−C−C (Pr)
	417 w	423 (4; 0)	427 (1; 1)	r N−Pr, r N−Me
			371 (2; 2)	δ N1-C−C (Pr
	363 w	359 (0; 0)	358 (0; 0)	δ N−Me, δ N−Pr, δ BF_4

TABLE 4: Continued

experiment (ν/cm^{-1}, I^a)		computations [ν, cm^{-1b} (I_{IR}, km/mole; I_{Ra}, Å^4·/AMU)]		assignments^c
IR neat (in CD_2Cl_2)	Raman	**11c**	**11a**	
	353 sh	354 (0; 0)	351 (0; 0)	δ BF_4
	318 w	325 (0; 1)		δ C−C−C
			304 (0; 1)	δ C−C−C
	281 w	281 (2; 1)	292 (2; 0)	γ N−Me, N−Pr
		249 (1; 1)	244 (0; 0)	δ N−Me, tors CH_3 (Pr)
	229 w	234 (2; 1)	232 (2; 2)	γ Me (out of plane)

[a] Labels: w, weak; m, medium; s, strong; v, very; sh, shoulder; br, broad. [b]SQM scaled wavenumbers. [c]Labels: ν, stretch; δ, bend; w, wagging; t, twisting; r, rocking; γ, out-of-plane; s, symmetrical; as, antisymmetrical.

too large to be ascribed to hydrogen bond formation, and the most important driving force of the association is, presumably, Coulomb attraction between the counterions.

(5) Vibrations of both the cations and the perfluoroanions are influenced not only by the association, but also by conformational changes of ethyl, propyl, butyl, or allyl groups bound to the imidazolium N-atom. The torsion energy potential surfaces of these groups depend on the nature of the anion and on its position relative to the cation. For example, two local minima corresponding to the planar and nonplanar ethyl groups relative to the imidazolium ring plane were found for the ethside structure of [EMIM][BF_4], although only the nonplanar conformer was observed for [EMIM][PF_6], or for the forward structure of [EMIM][BF_4]. These examples demonstrate that conformational or spectroscopic analysis of ILs on the basis of computations of the isolated cations may not adequately describe the system.

(6) Propyl and butyl groups bound to the imidazolium N-atom may adopt all the usual set of staggered *anti*- and *gauche*-conformations. The *gauche*-conformation of the propyl group and *gauche*,*gauche*-conformation of the butyl group, not previously discussed in the literature, were found to exist in [PMIM][BF_4] and [BMIM][BF_4], respectively.

Structure−Property Relationships. It is well known that vibrational characteristics of crystals predetermine their thermal properties.[54] Among these properties, the melting point is one of the most important physical properties to predict. In view of the difficulty of rationalizing the dependence of the melting point on chemical structure and the increasing need to predict the properties of yet unsynthesised ILs, calculations have been performed. An empirical method, quantitative structure−property relationship (QSPR),[55] has been used previously to predict IL melting points on the basis of the topology of molecules. However, the intrinsic relationship between the microstructure and the property cannot be revealed in this way. Some promise has been gained using ab initio HF and MP2 calculations to evaluate the interaction energy (E_{int}) of 1-alkyl-3-methylimidazolium halides.[9] The calculated E_{int} of the iodide series was found to increase with decreasing alkyl chain length, which was associated with an increase in the melting point. However, no trend was found for the corresponding bromide and chloride series. Moreover, detailed MP2/6-311G** ab initio computations of nine IL ion pairs clearly demonstrated that there is no close relationship between the calculated E_{int} and the melting point.[31]

Consequently, there is currently no method available to predict or rationalize the melting points of the approximately 10^{18} combinations of ions that could lead to useful ILs. We attempt to begin the process of redressing this situation by correlating the melting point with the structures and anharmonic vibrations of imidazolium-based ILs. Naturally, crystallized ILs represent too complex systems for direct calculation of their anharmonic vibrations, thus instead of the crystal, we consider an isolated ion pair regarded as an anharmonic oscillator. Accordingly, the anharmonic oscillator model from statistical mechanics is described in the first instance.

Consider the potential energy of the anharmonic oscillator

$$V(x) = \frac{m\omega^2}{2}x^2 - \frac{\beta}{3}x^3 \tag{1}$$

where $\omega = \sqrt{\alpha/m}$, m is the reduced mass of the oscillator, $\alpha = (\partial^2 E/\partial x^2)_0$ is the force constant of the oscillator, and $\beta = (\partial^3 E/\partial x^3)_0$ is the coefficient of anharmonicity of the oscillator.

Because of anharmonicity, when the temperature increases the mean position of the oscillation shifts from the equilibrium position by an amount a. The free energy of the anharmonic oscillator is given by[56]

$$F \le F_0 + \frac{m\omega^2}{2}a^2 - \frac{\beta}{3}a^3 - \beta a\langle y^2\rangle_0 \tag{2}$$

where a denotes the above mentioned shift from equilibrium, $y = x - a$, and

$$\langle y^2\rangle_0 = \frac{\hbar}{2m\omega}cth\left(\frac{\hbar\omega}{2kT}\right)$$

The value of a can be found from the condition of the minimum free energy with respect to a, i.e., from

$$m\omega^2 a - \beta a^2 - \beta\langle y^2\rangle_0 = 0 \tag{3}$$

The physically meaningful root of eq 3 is[57]

$$a = \frac{m\omega^2}{2\beta}\left(1 + \sqrt{1 - \left(\frac{\alpha\beta}{m\omega^2}\right)^2\langle y^2\rangle_0}\right)$$

In the case of

$$\left(\frac{m\omega^2}{2\beta}\right)^2 \le \frac{\hbar}{2m\omega}cth\left(\frac{\hbar\omega}{2kT}\right) \tag{4}$$

the system under consideration loses its stability, i.e., melts. The critical temperature, T_c, at which the loss of stability occurs can be found from the following equation:

$$T_c = \frac{\hbar\omega}{k\ln\dfrac{A+1}{A-1}} \tag{5}$$

where $A = 2m\omega/\hbar(m\omega^2/2\beta)^2$

Because at T_c the first derivative of the free energy (eq 3) tends to ∞, T_c is the point of the phase transition of the first kind (in our case it is the melting point T_{mp}).

TABLE 5: Vibrational Spectra of [BMIM][BF_4]

experiment (ν/cm^{-1}, I^a)		computations [ν, cm^{-1b} (I_{IR}, km/mole; I_{Ra}, Å^4/AMU)]						assignments^c
IR neat (CD_2Cl_2)	Raman	**7g** (ga)	**7c** (-ga)	**7a** (aa)	**7f** (-gg)	**7h** (gg)	**7i** (g-g)	
3163 s (3163 s)	3173 w	3179 (1; 94)	3180 (0; 94)	3178 (0; 103)	3183 (1; 85)	3179 (1; 93)	3178 (1; 101)	ν C4−H, C5−H (in-phase)
	3157 sh	3162 (5; 49)	3162 (5; 52)	3160 (5; 52)	3163 (4; 54)	3161 (5; 49)	3161 (5; 51)	νC4−H,C5−H (out-of-phase)
3123 s (3123 s)	3127 wv	3132 (210; 44)	3150 (191; 38)	3152 (195; 34)	3123 (226; 47)	3131 (212; 46)	3122 (245; 91)	ν C2−H
3105 sh (3105 sh)	3112 w							
	3030 sh	3020 (17; 35)	3007 (17; 38)	3004 (12; 39)	3019 (4; 33)	3019 (16; 36)	3017 (46; 22)	ν_{as} CH_3 (Me)
	3001 sh	2992 (7; 71)	2983 (1; 32)	2992 (1; 25)	2989 (7; 72)	2990 (7; 75)	2982 (9; 76)	ν_{as} CH_3 (Me)
2966 s (2966 s)	2969 vs	2963 (5; 47)	2983 (8; 76)	2981 (8; 79)	2978 (0; 33)	2969 (4; 41)	2957 (5; 37)	ν_{as} CH_2
		2947 (16; 71)	2949 (27; 12)	2948 (6; 26)	2976 (4; 34)	2949 (12; 58)	2952 (0; 35)	ν_{as} CH_3, CH_2
2942 s (2942 s)	2942 s	2943 (30; 29)	2943 (27; 72)	2943 (31; 68)	2934 (23; 34)	2939 (30; 79)	2939 (20; 50)	ν_{as} CH_2
		2936 (30; 50)	2912 (24; 64)	2933 (41; 49)	2923 (23; 92)	2925 (74; 12)	2932 (56; 70)	ν_{as} CH_3, CH_2
	2917 s	2911 (34; 158)	2907 (26; 48)	2910 (29; 110)	2912 (28; 155)	2918 (30; 138)	2905 (30; 129)	ν_s CH_3 (Me)
		2907 (27; 106)	2906 (18; 166)	2904 (35; 159)	2902 (51; 194)	2910 (35; 152)	2903 (50; 149)	ν_s CH_3 (Me)
				2902 (12; 65)		2901 (2; 91)	2894 (21; 107)	ν_{as} CH_2
					2890 (22; 73)			ν_s CH_3 (Me)
2878 m (2878 m)	2877 s	2888 (46; 37)	2905 (39; 149)					ν_s CH_2
		2875 (25; 129)	2886 (18; 99)	2871 (33; 125)	2869 (38; 147)	2876 (47; 16)	2877 (17; 57)	ν_s CH_3 (Bu)
		2869 (8; 119)	2863 (39; 122)	2857 (26; 50)	2863 (35; 70)	2867 (1; 212)	2874 (35; 170)	ν_s CH_2
					2853 (21; 43)	2865 (20; 70)	2844 (50; 84)	ν_s CH_3 (Bu)
	2840 w	2840 (39; 80)	2850 (24; 58)	2849 (39; 92)				ν_s CH_2
1618 sh (1618 sh)								
1575 s (1575 s)	1568 w	1584 (20; 3)	1584 (21; 4)	1581 (20; 4)	1584 (35; 2)	1584 (20; 3)	1583 (16; 3)	ν C=C
1568 sh (1568 sh)		1566 (46; 2)	1572 (49; 2)	1571 (51; 2)	1575 (35; 3)	1566 (45; 3)	1563 (42; 3)	ν_{as} N1C2N3, r C2H
				1472 (4; 3)	1473 (12; 8)		1488 (9; 7)	δ_{as} CH_3 (Bu), CH_2
1467 s (1467 s)	1464 sh	1470 (5; 6)	1474 (7; 20)	1470 (10; 17)	1471 (7; 18)	1470 (3; 6)		δ_s CH_3
1459 sh (1459 sh)		1468 (11; 16)	1464 (8; 8)	1460 (9; 19)	1459 (6; 10)	1463 (10; 12)	1476 (9; 14)	δ_{as} CH_3 (Me)
				1460 (2; 4)		1462 (17; 13)	1474 (14; 9)	δ_{as} CH_3 (Me)
1454 sh (1454 sh)	1448 m	1457 (6; 17)	1458 (7; 18)		1459 (8; 9)		1471 (7; 13)	δ_{as} CH_3 (Bu)
		1455 (2; 4)	1458 (13; 13)	1455 (7; 17)		1455 (11; 5)		δ_s CH_2
		1453 (16; 12)	1457 (1; 13)	1454 (2; 43)	1450 (11; 16)	1452 (8; 22)	1457 (4; 7)	δ_{as} CH_3 (Me)
		1449 (2; 23)	1446 (19; 3)	1451 (6; 1)	1448 (15; 16)	1450 (4; 16)	1454 (8; 22)	δ_s CH_2
		1447 (12; 18)	1439 (4; 26)		1440 (3; 14)	1446 (7; 27)	1446 (4; 18)	δ_s CH_2
1431 m (1431 m)	1421 m	1431 (12; 12)	1433 (12; 17)	1430 (10; 16)	1432 (10; 15)	1431 (12; 12)	1432 (10; 13)	δ_s CH_3 (Me)
		1420 (4; 27)	1421 (3; 26)	1419 (4; 33)	1421 (5; 21)	1420 (5; 26)	1417 (6; 16)	δ CH_2, ν ring
		1398 (2; 3)	1399 (1; 5)	1397 (4; 3)	1397 (3; 5)	1399 (5; 8)	1407 (2; 12)	δ_s CH_3 (Bu)
1387 m (1387 m)	1391 m	1387 (0; 11)	1388 (6; 9)	1387 (8; 3)	1391 (5; 13)	1383 (1; 10)	1395 (2; 12)	w CH_2
1373 sh (1373 sh)		1375 (5; 3)	1387 (4; 1)	1380 (2; 6)	1378 (7; 3)	1379 (6; 3)	1369 (2; 5)	ν_{as}C2N1C5, w CH_2
1363 sh		1367 (19; 11)	1361 (7; 2)	1361 (1; 2)	1366 (4; 4)	1369 (7; 6)	1367 (15; 7)	w CH_2
					1364 (8; 1)			w CH_2
1339 m (1339 m)	1342 m	1334 (3; 18)	1330 (9; 18)	1332 (7; 32)		1347 (11; 1)	1359 (11; 6)	ν N−Bu, N−Me, breathing, w CH_2
	1311 w	1315 (9; 9)	1328 (4; 9)	1318 (1; 10)	1320 (7; 29)	1322 (11; 26)	1320 (9; 18)	
1300 vw	1303 w	1308 (3; 13)	1310 (4; 13)	1304 (2; 3)	1312 (1; 4)	1304 (1; 11)	1293 (2; 3)	t CH_2
	1286 vw	1282 (2; 1)	1279 (2; 4)	1287 (7; 6)	1287 (4; 4)	1279 (3; 3)	1280 (7; 6)	r C−H, t CH_2
				1273 (4; 2)	1270 (7; 8)		1273 (2; 7)	r C−H, t CH_2
1285 s (1285 s)		1254 (211; 2)	1253 (155; 2)	1247 (451; 0)	1222 (449; 0)	1246 (445; 0)	1255 (433; 0)	ν BF_4, t CH_2
1253 sh (1253 sh)	1254 vw	1258 (3; 4)	1260 (3; 9)	1256 (10; 2)	1257 (32; 2)	1255 (3; 5)		t CH_2, r C2−H
1213 w (1213 w)	1212 vw	1214 (279; 2)	1218 (314;)				1222 (72; 1)	ν BF_4, t CH_2
						1199 (46; 3)		r C2-H, t CH_2
1172 vs (1172 vs)	1173 vw	1159 (178; 1)	1158 (185; 2)	1153 (163; 2)	1165 (172; 2)	1156 (179; 1)	1157 (151; 3)	ν N−Bu, N−Me, rCH
	1148 sh	1142 (1; 2)	1143 (10; 3)	1143 (35; 4)	1140 (1; 3)	1143 (3; 2)	1149 (8; 3)	r CH_3
	1132 vw	1136 (3; 3)	1124 (4; 1)	1140 (6; 2)	1136 (10; 0)	1123 (4; 2)	1129 (19; 2)	r CH_2 (Bu)

TABLE 5: Continued

experiment (ν/cm^{-1}, I^a)		computations [ν, cm^{-1b} (I_{IR}, km/mole; I_{Ra}, Å^4/AMU)]						assignments^c
IR neat (CD_2Cl_2)	Raman	**7g** (ga)	**7c** (-ga)	**7a** (aa)	**7f** (-gg)	**7h** (gg)	**7i** (g-g)	
1116 sh	1117 m	1113 (8; 5)	1110 (10; 1)	1116 (3; 6)		1109 (12; 3)	1103 (9; 4)	r CH_3, r CH_3 (Bu)
(1116 sh)								
		1101 (3; 1)	1103 (8; 3)	1102 (11; 5)	1106 (4; 2)	1093 (1; 2)	1096 (7; 6)	r CH_3, r CH_3 (Bu)
	1093 w	1091 (9; 6)	1091 (10; 6)		1091 (9; 6)	1090 (12; 6)	1091 (1; 2)	r C−H
1074 vs broad		1084 (186; 1)	1069 (16; 7)	1089 (15; 7)	1084 (1; 5)	1085 (50; 1)	1074 (4; 8)	ν C−C, ν BF_4
(1074 broad)								
					1066 (5; 2)			ν C−C
				1071 (26; 7)	1065 (158; 1)	1051 (168; 1)	1060 (211; 0)	ν BF_4, ν C−C, r C−H
1037 sh	1057 m	1039 (37; 10)	1046 (162; 0)	1042 (164; 1)	1040 (56; 3)			ν C−C, ν BF
(1037 sh)								
		1025 (25; 3)	1022 (28; 6)	1028 (45; 4)		1029 (23; 4)	1036 (55; 4)	δ ring
		1016 (24; 11)	1015 (19; 10)	1015 (25; 8)	1020 (33; 8)	1016 (31; 12)	1019 (28; 4)	breathing, νN−Bu, νN−Me
1019 sh	1024 vw	1006 (237; 0)	1003 (62; 1)	1001 (5; 1)	1002 (148; 1)	1004 (236; 1)	1011 (221; 2)	ν BF_4
(1019 sh)								
992 sh				983 (161; 1)	982 (112; 1)			ν BF_4, γ C−H
(992 sh)								
(975 sh)	976 w	965 (7; 1)	976 (169; 1)	968 (105; 0)	960 (32; 4)	958 (1; 3)	954 (1; 1)	ν_{as} C−C
(948 w)	951 w	945 (7; 1)	973 (72; 1/)					r CH_3 (Bu), CH_2
(941 sh)		930 (30; 1)	946 (1; 0)	937 (2; 1)	935 (10; 1)	937 (3; 4)	931 (1; 1)	γ *C*2-H
						926 (33; 1)	929 (33; 2)	γ *C*2-H
(903 w)	907 m							
(893 w)				894 (3; 8)	874 (4; 1)			ν C−C
(875 sh)	884 m	875 (3; 2)	870 (0; 1)			871 (5; 2)	878 (10; 1)	ν C−C
(852 sh)								
(849 s)		815(0; 1)	815 (1; 7)	813 (0; 0)	814 (0; 0)	814 (0; 0)	814 (0; 0)	γ C4-H, C5-H
(835 sh)	825 m	807 (0; 7)	805 (0; 1)					ν_s C−C−C
(808 w)	810 m			796 (1; 1)	795 (2; 5)	785 (3; 9)	794 (2; 6)	ν_s C−C−C
(762 sh s)	765 s	758 (9; 3)	756 (9; 3)	756 (6; 2)	762 (14; 3)	758 (10; 1)	764 (5; 2)	ν_s BF_4
(755 s)		749 (8; 1)		741 (20; 1)	756 (10; 3)	743 (10; 3)	760 (10; 3)	r CH_2
(737 sh)	734 w		731 (9; 1)					r CH_2
		724 (34; 2)	723 (28; 2)	722 (29; 2)	723 (30; 2)	723 (34; 2)	724 (37; 2)	γ C4-H, C5-H
				724 (9; 2)				ν N−Me, ν N−Bu
(697 m)	699 m	692 (8; 2)	687 (10; 2)		686 (9; 2)	692 (6; 2)	690 (8; 2)	ν N−Me, ν N−Bu
(660 sh)	658 m			672 (35; 2)				ν N−Me, ν N−Bu
(652 s)		666 (27; 0)	666 (40; 0)		662 (37; 0)	667 (28; 0)	656 (24; 0)	γ N−Me, γ N−Bu
(623 s)	624 m	627 (5; 0)	628 (2; 1)	634 (7; 3)	626 (2; 1)	628 (5; 1)	625 (2; 1)	γ N−Bu, ring-packering
				618 (1; 3)				
(601 m)	601 m	589 (1; 5)	594 (0; 5)		589 (0; 5)	591 (1; 5)	582 (1; 5)	δ N1−C2-N3
(535 sh)								
(520 s)	521 m	526 (20; 1)	526 (20; 1)	524 (19; 1)	526 (21; 1)	526 (21; 1)	525 (21; 1)	δ BF_4
		517 (4; 0)	515 (3; 0)	514 (4; 0)	516 (2; 0)	517 (4; 0)	519 (3; 0)	δ BF_4
		510 (2; 0)	510 (3; 0)	512 (1; 0)	510 (3; 0)	510 (2; 0)	513 (1;0)	δ BF_4
	501 w	492 (1; 1)	499 (0; 2)				481 (2; 1)	δ N−C−C, C−C−C
	473 w				476 (1; 2)	465 (1; 1)		δ N−C−C, C−C−C
	435 w			442 (1; 1)				r N−Bu, r N−Me, δ N−C−C, C−C−C
	415 m	424 (4; 0)	422 (3; 1)	415 (2; 0)	421 (2; 1)	422 (4; 0)	422 (4; 0)	r N−Bu, r N−Me
	392 w					398 (1; 1)		r N−Bu, r N−Me, δ C−C−C
	352 m	358 (1; 0)	356 (0; 0)	357 (0; 0)	357 (1; 0)	358 (1; 0)	360 (1; 0)	δ N−Me, δ N−Bu, δ BF_4
		352 (0; 0)	354 (0; 0)	351 (0; 0)	354 (0; 0)	353 (0; 0)	351 (1; 0)	δ BF_4
					341 (1; 0)		350 (0; 0)	δ C−C−C
	325 m	328 (1; 1)	319 (4; 2)	326 (2; 3)	321 (5; 1)		329 (1; 1)	δ C−C−C
	298 sh	296 (3; 1)	302 (1; 0)			307 (1; 0)		r N−Me, N−Bu
	282 m			294 (3; 0)	274 (0; 1)	283 (1; 1)	285 (3; 1)	tors Bu
	257 m	256 (1; 1)	251 (1; 1)	250 (1; 1)	246 (3; 1)		268 (1; 1)	γ N−Me, δ C−C−C
	240 w	245 (0; 0)	241 (1; 0)	239 (0; 0)	239 (1; 1)	242 (2; 1)	239 (3; 1)	tors CH_3 (Bu)
	212 w	218 (2; 1)	231 (4; 1)	215 (2; 1)		207 (1; 1)		δ C−C−C

[a] Labels: w, weak; m, medium; s, strong; v, very; sh, shoulder; br, broad. [b]SQM scaled wavenumbers. [c]Labels: ν, stretch; δ, bend; w, wagging; t, twisting; r, rocking; γ, out-of-plane; s, symmetrical; as, antisymmetrical.

At A → 1, T_{mp} → 0, but the case of practical interest is A ≫ 1. Then,

$$\ln\frac{A+1}{A-1} = 2\sum_{n=0}^{\infty}\frac{1}{(2n+1)}A^{2n+1} = 2\left(\frac{1}{A}+\frac{1}{3A^3}+\frac{1}{5A^5}+...\right) \approx \frac{2}{A}$$

Hence,

$$T_{mp} = \frac{m\omega^2}{k}\left(\frac{m\omega^2}{2\beta}\right)^2 = \frac{\alpha}{k}\left(\frac{\alpha}{2\beta}\right)^2 = \frac{1}{4k}\cdot\frac{\alpha^3}{\beta^2} \qquad (6)$$

Evaluation of Quasy-Elastic Characteristics α and β and Their Interrelation with Melting Point. As shown above, [EMIM][Halide] ILs cannot be regarded as consisting of ion

TABLE 6: Vibrational Spectra of [AMIM][BF_4]

experiment (ν/cm^{-1}, I^a)		computations [ν, cm^{-1b} (I_{IR}, km/mole; I_{Ra}, Å^4/AMU)]		assignments^c
IR	Raman	**12a**	**12c**	
3163 s	3175 w	3181 (2; 85)	3182 (1; 93)	ν C4−H,C5−H (in-phase)
		3163 (5; 53)	3163 (4; 56)	ν C4−H,C5−H (out-of-phase)
3122 s	3128 vvw	3128 (230; 48)	3131 (262; 50)	ν C2-H
3104 sh	3097 m	3102 (10; 83)	3114 (5; 52)	ν_{as} CH_2 (C═C)
	3030 s	3069 (6; 55)	3031 (12; 40)	ν CH (C═C)
		3019 (9; 41)	3021 (30; 149)	ν_s CH_2 (C═C)
2998 w sh	2996 s	3006 (11; 77)	3006 (8; 72)	ν_{as} CH_3
	2971 vs	2983 (8; 99)	2981 (11; 63)	ν_{as} CH_3
2962 m	2971 sh	2967 (7; 48)	2972 (16; 50)	ν_{as} CH_2
		2907 (27; 107)	2909 (26; 117)	ν_s CH_2
		2905 (35; 154)	2904 (35; 152)	ν_s CH_3
1648 m	1648 vs	1665 (2; 23)	1653 (0; 19)	ν C═C
1575 s	1576 sh	1582 (25; 3)	1581 (23; 3)	ν C═C (ring)
1566 s	1567 m	1569 (57; 2)	1567 (43; 3)	ν_{as} N1C2N3, r C2H
	1495 w sh			
1479 sh	1473 w sh	1467 (11; 17)	1469 (7; 18)	δ_{as} CH_3 (Me)
		1460 (7; 23)	1460 (7; 20)	δ_{as} CH_3 (Me)
1452 m	1453 m	1454 (7; 10)	1466 (10; 10)	δ_{as} CH_2
1426 m	1433 sh	1428 (2; 6)	1429 (15; 14)	δ_s CH_3 (Me)
		1427 (31; 24)	1439 (5; 9)	δ CH_2 (C═C)
1413 sh	1416 s	1417 (1; 27)	1410 (3; 21)	δ CH_2, CH_2(C═C)
1388 m	1387 m	1385 (5; 10)	1388 (5; 17)	ν_{as}C2N1C5
1346 m br	1349 sh	1349 (7; 1)	1355 (5; 2)	w CH_2
1329 m br	1329 m br			
			1313 (1; 12)	r CH (C═C)
1295 sh	1296 m	1307 (9; 31)	1299 (15; 18)	ν_s N−A, N−Me, breathing
1287 m		1290 (0; 21)		r CH (C═C)
1268 sh	1273 sh	1281 (1; 2)	1289 (4; 6)	r CH (ring)
1260 s	1251 w	1257 (475;)	1258 (476; 0)	ν BF_4
	1222 w	1232 (12; 8)	1241 (13; 5)	t CH_2
	1207 sh			
1173 sh	1181 w			
1168 s	1167 m	1154 (149; 1)	1150 (155; 3)	r CH (ring)
	1140 w	1144 (2; 3)	1143 (22; 4)	r CH_3
	1138 w	1141 (56; 3)	1134 (46; 1)	ν C−C, r CH_3
1115 sh	1114 m	1099 (9; 4)	1101 (12; 4)	r CH_3
1090 sh	1091 m	1088 (14; 6)	1090 (14; 6)	r CH (ring)
	1077 vw sh	1073 (110; 3)	1075 (178; 1)	r CH, t CH_2 (C═C)
1057 vvs		1049 (150; 1)	1041 (103; 2)	t CH_2 (C═C), r CH
1038 vvs		1038 (38; 2)	1033 (23; 3)	δ ring
1019 vvs	1022 vs	1018 (25; 11)	1014 (31; 10)	breathing, νN−A, νN−Me
			997 (0; 1)	γ C2-H
993 sh	999 vw sh	995 (119; 2)	991 (137; 1)	ν BF_4
	970 sh			
		956 (48; 2)		γ C2-H, ν C−C
950 m	953 m	953 (34; 0)		w CH_2 (C═C)
			925 (6; 5)	ν C−C
920 sh	919 m	910 (11; 2)	922 (2; 1)	r CH_2 (C═C)
873 sh	872 w			
862 sh	862 w	970 (99; 2)	985 (106; 1)	γ C2-H
851 s				
841 sh	830 w			
816 sh	816 w	816 (0; 0)	813 (0; 0)	γ C4−H, C5−H
792 s				
782 m				
770 m				
756 m	767 vs	757 (11; 3)	758 (10; 3)	ν_s BF_4
748 s	750 w sh	761 (15; 4)	776 (25; 8)	ν N−A
745 sh				
	725 vw	722 (30; 2)	720 (34; 2)	γ C4−H, C5−H
	676 vs	678 (13; 3)	678 (12; 3)	ν N−Me
	664 sh	654 (37; 3)	652 (25; 2)	γ N−Me, N−A
	625 vs	620 (0; 3)	618 (0; 3)	γ N−Me, N−A, ring-packering
	570 vs	571 (3; 6)		δ N1−C2-N3
			539 (1; 4)	δ N1−C2-N3
	522 m	524 (21; 1)	524 (20; 1)	δ BF_4
		515 (2; 1)	516 (2; 0)	δ BF_4
	509 m	509 (1; 0)	511 (1; 0)	δ BF_4
			461 (3; 3)	δ C−C═C
	441 sh			
	423 m	435 (3; 1)	420 (3; 1)	r N−A, r N−Me

TABLE 6: Continued

experiment (ν/cm^{-1}, I^a)		computations [ν, cm^{-1b} (I_{IR}, km/mole; I_{Ra}, Å^4/AMU)]		assignments^c
IR	Raman	**12a**	**12c**	
	396 s	395 (0; 3)		δ C−C=C
	364 sh	361 (1; 1)		γ N−Me, N−A
	353 m	357 (0; 0)	357 (0; 0)	δ BF_4
		351 (0; 0)	351 (0; 0)	δ BF_4
			329 (3; 3)	γ N−Me, N−A
	268 m	272 (1; 2)	274 (0; 0)	δ N−Me, N−A
	233 m	233 (2; 1)	226 (1; 2)	γ N−Me, ring packering

[a] Labels: w, weak; m, medium; s, strong; v, very; sh, shoulder; br, broad. [b]SQM scaled wavenumbers. [c]Labels: ν, stretch; δ, bend; w, wagging; t, twisting; r, rocking; γ, out-of-plane; s, symmetrical; as, antisymmetrical.

pairs because each cation is H-bonded via C2−H, C4−H, and C5−H bonds to three anions, and each anion is bonded to three cations.[6−8] In contrast, the BF_4^- or PF_6^- anions in all the ILs studied adopt the position close to the C2-atom of imidazolium, although the presence of minor forms corresponding to the anion near C4 or C5 atoms cannot be excluded. This means that, to a first approximation, ion pairs can be regarded as the major structural form of these ILs. In the ILs **6**, **9**, **10**, **12**, and **13** this major form corresponds to the global minimum of the energy surface of the isolated ion pair. The liquid state of **11** adopts structure **11c** (Figure 4), whereas liquid **7** contains at least two local-minimum structures **7g** and **7h** (Figure 5), and the global-minimum structure **7a** cannot be excluded. It is quite possible that the minima populated in crystals differ from both global and local minima populated in the liquid state, as is the case for **6**.[38] The crystal of **13** exists in the form[37] coinciding with the local-minimum structure **13b** (Figure 7). Thus, the melting points of **6** and **13** were calculated using eq 6 for **6h** and **13b**, respectively. To evaluate the influence of various modes of binding between the counterions on melting point, we calculated T_{mp} also for the global-minimum ion pairs **6a** and **13a**. In the absence of X-ray data on other studied ILs, T_{mp} was calculated for global-minimum ion pairs and for several additional local-minimum structures.

For this purpose, the distance R between the center of the anion and C2 of the cation was selected as the internal coordinate x in eq 1. In the case of **6h** exclusively, the distance between the center of the anion and C5 of the cation was regarded as x. To evaluate the dependence of E on R, the potential energy surface of the ion pair was scanned in the vicinity of its minimum. R was initially set at its equilibrium value, obtained after geometry optimization, and was stepped four times by 0.1 Å toward smaller values and once toward a higher value. All the internal coordinates except R were allowed to relax at every step. The resulting six points were interpolated by a polynomial of degree 3: $E = A + BR + CR^2 + DR^3$. C was taken as $\alpha/2$, and D was taken as $\beta/3$ (see eqs 1 and 6).

This approach, apart from using a rather simplified theoretical model, is based on two additional assumptions: (i) "interionic" vibration, described by the above mentioned internal coordinate R, is regarded as a pure mode that does not mix with "intraionic" vibrations and (ii) the influence of the surrounding medium on the anharmonic oscillator is not taken into account. Such assumptions mean that it is not possible that T_{mp} from eq 6 will match the corresponding experimental values quantitatively, but the qualitative trends should be modeled.

The parameters α^3/β^2 (eq 6) are summarized together with the calculated interaction energy E_{int} of the ion pairs **6**, **7**, and **9-13** in Table 7. A close relation between the E_{int} and the experimental melting points is absent, which indicates that melting points are not determined by the value of $E_{int.}$ The calculated α^3/β^2 values are sensitive to structural changes in **6**, **7**, and **9-13**. Thus, the results of their analysis depend on the structures chosen for comparison with the experiment. In the absence of X-ray data for ILs **7** and **9-12**, we assumed that they crystallize in the forms that dominate in the liquid state (as indicated by IR and Raman spectroscopy). Computed α^3/β^2 values for these forms follow the experimentally determined trend: T_{mp}(**13**) > T_{mp}(**10**) > T_{mp}(**9**) > T_{mp}(**6**) > T_{mp}(**11**) > T_{mp}(**12**). It should be noted that α^3/β^2 of **12a** is higher than the corresponding value calculated for **11c**. The calculations for **12c** fit more closely with the above mentioned experimental trend (Table 7). Possibly, the reason is that **12** crystallizes in the form **12c** instead of in the form **12a**, which is believed to dominate in the liquid state.

TABLE 7: Melting Points (mp), Interaction Energies (E_{int}) and Quasi-Elastic Parameters (α^3/β^2) of Ionic Liquids 6−7, 9−13

ionic liquid		mp/K	E_{int}/kcal/mol^{-1}	α^3/β^2/H
[EMIM][PF_6]	**13a**	340	88.5	0.149
	13b		87.1	0.374[a]
[EDMIM][BF_4]	**10a**	301	93.0	0.285[a]
[DMIM][BF_4]	**9a**	283	96.4	0.094[a]
[EMIM][BF_4]	**6a**	279	97.0	0.052
	6h	272[b]	86.3	0.023
[PMIM][BF_4]	**11c**	231	95.7	0.021[a]
	11a		96.6	0.015
[BMIM][BF_4]	**7a**	194[c]	96.4	0.028
	7f		97.4	0.115
	7g		95.9	0.018
	7h		95.3	0.017
	7i		96.7	0.068
[AMIM][BF_4]	**12a**	192	97.1	0.051[a]
	12c		*d*	0.019

[a] The values which are to be compared with the experimental melting points. They belong to structures dominant either in the liquid or crystalline states (see text); [b]This melting point does not correspond to that of the crystal but the of the impure commercially purchased product prior to crystallization. [c] This temperature corresponds to glass transition, which cannot be rationalized within the framework of the model used. Nevertheless, it may be regarded as an indication of a low melting point. [d]E_{int} cannot be evaluated because the isolated cation $AMIM^+$ adopts conformation different from **12c**.

Overall, the experimental melting points correlate with quasy-elastic characteristics α^3/β^2 of **6**, **7**, and **9-13** much more closely than with their interaction energies. In particular, our approach correctly predicts a higher melting point of [EMIM][PF_6] in comparison with [EMIM][BF_4], and lowering of the melting point when the ethyl group in [EMIM][BF_4] is replaced by the propyl group in [PMIM][BF_4], and the experimentally observed increase of T_{mp} that is caused by the replacement of H2 in [EMIM][BF_4] by the methyl group in [EDMIM][BF_4]. In this latter case, one might expect a lower melting point rather than a higher one for [EDMIM][BF_4], because the most acidic H2 proton in [EMIM][BF_4] is replaced by a methyl group, and hence the hydrogen bonding between the [EDMIM] and [BF_4]

is either absent or very weak in comparison with [EMIM][BF_4]. Within the framework of our approach this case is not an anomaly; it merely has to be explained in terms of quasy-elastic characteristics of the counterions instead of their H-bonds.

It is interesting to note that according to Table 7 conformational transformations of the side chain bound to the N1 atom of the imidazolium ring may influence T_{mp} even to a greater extent than the above mentioned dramatic changes of molecular structure. For example, **7g** or **7h** conformers of [BMIM][BF_4] should have a much lower melting point than the conformer **7f**. The T_{mp} of **7f** is expected to be even higher than T_{mp} of [DMIM][BF_4]. Additionally, the predicted difference in the melting points of the front (**6a**) and methside (**6h**) forms of [EMIM][BF_4] is not so pronounced; according to Table 7, the T_{mp} for both forms should be expected between melting points of [PMIM][BF_4] and [DMIM][BF_4].

This latter case demonstrates that our approach can be used for the evaluation of T_{mp} of yet unsynthesised ILs through the computation of their quasi-elastic characteristics α^3/β^2 and comparison with the corresponding parameters of the ILs with known melting points. These evaluations would be especially efficient for the prediction of high melting points because α^3/β^2 values differ essentially for ILs with T_{mp} around (or higher than) ambient temperature (cf. [MMIM][BF_4], [EDMIM][BF_4], and [EMIM][PF_6] in Table 7). For melting points below 0 °C, evaluations of this kind would be much less reliable because α^3/β^2 values depend on T_{mp} only slightly.

Conclusions

In summary, the combined DFT−vibrational spectroscopy approach allows both common features and differences in structure of various imidazolium-based ILs to be revealed. It is shown that both the halides and the perfluorinated anions are able to occupy forward, side, and back positions around the imidazolium ring, but the former populate all three positions essentially to an equal extent, while the latter prefer the forward position. Ethyl, propyl, butyl, or allyl groups bound to the imidazolium N-atom of the isolated cation adopt all the usual set of staggered or eclipsed conformations well known from organic chemistry, but the relative concentrations of various conformers may strongly depend on the type and position of the anion. Vibrations of the cations depend not only on the conformational changes, but also on the association with the counterions. The formation of the associates influences mainly stretching and out-of-plane vibrations of the imidazolium C−H groups and stretching vibrations of the perfluoroanions. Other modes of the counterions retain their individuality and practically do not mix. This allows "interionic" vibrations to be separated, and the couple of the ion pair can be regarded as an anharmonic oscillator. This simple model correlates the molecular structure of various ILs and their melting points and offers an explanation for the experimental observations in the melting point dependence on the structure of the ILs without involving the energy of the interaction between the cations and anions but on the grounds of their quasi-elastic properties. Our preliminary investigation of a series of six cations paired with two anions provides some initial hints as to the relationship between structure, vibrations, and melting point. We are striving to refine correlations and improve on our models to overcome the limitations of the methods used thus far.

Acknowledgment. The financial support of the Swiss National Science Foundation (SCOPES) and the Russian Science Support Foundation (EEZ) is gratefully acknowledged. We thank Dr. J. Slattery for recording the Raman spectra of the compounds, and Dr. M. A. Tafipolsky for permission to use his version of the program, adopted from Sipachev.[44]

Supporting Information Available: Scaling factors used in this work, vibrational spectra of [DMIM][BF_4] and [EDMIM][BF_4], and SQM vibrational spectra of BF_4^- and PF_6^-. This material is available free of charge via the Internet at http://pubs.acs.org.

References and Notes

(1) (a) Chum, H. L.; Koch, V. R.; Miller, L. L.; Osteryoung, R. A. *J. Am. Chem. Soc*. **1975**, *97*, 3264−3265. (b) Robinson, J.; Osteryoung, R. A. *J. Am. Chem. Soc*. **1979**, *101*, 323−327. (c) Wilkes, J. S.; Levisky, J. A.; Wilson, R. A.; Hussey, C. L. *Inorg. Chem*. **1982**, *21*, 1263−1264. (d) Scheffler, T. B.; Hussey, C. L.; Seddon, K. R.; Kear, C. M.; Armitage, P. D. *Inorg. Chem.* **1983**, *22*, 2099−2100. (e) Appleby, D.; Hussey, C. L.; Seddon, K. R.; Turp, J. E. *Nature* **1986**, *323*, 614−616. (f) Boon, J. A.; Levisky, J. A.; Pflug, J. L.; Wilkes, J. S. *J. Org. Chem.* **1986**, *51*, 480−483.

(2) (a) Wilkes, J. S.; Zaworotko, M. J. *J. Chem. Soc., Chem. Commun.* **1992**, 965−967. (b) Bonhôte, P.; Dias, A. P.; Papageorgiou, N.; Kalyanasundaram, K.; Grätzel, M. *Inorg. Chem.* **1996**, *35*, 1168−1178.

(3) (a) Seddon, K. R. *J. Chem. Technol. Biotechnol.* **1997**, *68*, 351−356. (b) Wasserscheid, P.; Keim, W. *Angew. Chem., Int. Ed.* **2000**, *39*, 3772−3789. (c) Zhao, D.; Wu, M.; Kou, Y.; Min, E. *Catal. Today* **2002**, *74*, 157−189. (d) Wang, P.; Zakeeruddin, S. M.; Comte, P.; Exnar, I.; Grätzel, M. *J. Am. Chem. Soc.* **2003**, *125*, 1166−1167. (e) Bates, E. D.; Mayton, R. D.; Ntai, I.; Davis J. H., Jr. *J. Am. Chem. Soc*. **2002**, *124*, 926−927. (f) Armstrong, D. W.; Zhang, L. K.; He, L. F.; Gross, M. L. *Anal. Chem*. **2001**, *73*, 3679−3686.

(4) *Ionic Liquid in Synthesis*; Wasserscheid, P., Welton, T., Eds.; Wiley-VCH: New York, **2002**; p 33.

(5) Holbrey, J. D.; Seddon, K. R. *Clean Prod. Process.* **1999**, *1*, 223−236.

(6) Dieter, K. M.; Dymek, C. M.; Heimer, N. E., Jr. ; Rowang, J. W.; Wilkes, J. S.; *J. Am. Chem. Soc.* **1988**, *110*, 2722−2726.

(7) Dymek, C. M.; Grossie, D. A., Jr.; Fratini, A. V.; Adams, W. W. *J. Mol. Struct.* **1989**, *213*, 25−34.

(8) Elaiwi, A.; Hitchcock, P. B.; Seddon, K. R.; Srinivasan, N.; Tan, Y. M.; Welton, T.; Zora, J. A. *J. Chem. Soc., Dalton Trans*. **1995**, 3467−3472.

(9) Turner, E. A.; Pye, C. C.; Singer, R. D. *J. Phys. Chem. A* **2003**, *107*, 2277−2288.

(10) Hunt, P. A.; Gould, I. R. *J. Phys. Chem. B* **2006**, *110*, 2269−2282.

(11) Hanke, C. G.; Price, S. L.; Linden-Bell, R. M. *Mol. Phys.* **2001**, *99*, 801−809.

(12) Hardacre, C.; McMath, S. E. J.; Nieuwenhuyzen, M.; Bowron, D. T.; Soper, A. K. *J. Phys.: Condens. Matter* **2003**, *15*, S159−S166.

(13) *Ionic Liquid in Synthesis*; Wasserscheid, P., Welton, T., Eds.; Wiley-VCH: New York, **2002**; p 133.

(14) Hardacre, C.; Holbrey, J. D.; McMath, S. E. J.; Bowron, D. T.; Soper, A. K. *J. Chem. Phys.* **2003**, *118*, 273−278.

(15) Del Popolo, M. G.; Lynden-Bell, R. M.; Kohanoff, J. *J. Phys. Chem. B* **2005**, *109*, 5895−5902.

(16) Bühl, M.; Chaumont, A.; Schurhammer, R.; Wipff, G. *J. Phys. Chem. B* **2005**, *109*, 18591−18599.

(17) Arduengo, A. J.; Dias, H. V. R.; Harlow, R. L.; Kline, M. *J. Am. Chem. Soc.* **1992**, *114*, 5530−5534.

(18) Avent, A. G.; Chaloner, P. A.; Day, M. P.; Seddon, K. R.; Welton, T. *J. Chem. Soc., Dalton Trans.* **1994**, 3405−3413.

(19) Ozawa, R.; Hayashi, S.; Saha, S.; Kobayashi, A.; Hamaguchi, H. *Chem. Lett.* **2003**, *32*, 948−949.

(20) Katayanagi, H.; Hayashi, S.; Hamaguchi, H. O.; Nishikawa, K. *Chem. Phys. Lett.* **2004**, *392*, 460−464.

(21) Saha, S.; Hayashi, S.; Kobayashi, A.; Hamaguchi, H. *Chem. Lett.* **2003**, *32*, 720−741.

(22) Hayashi, S.; Ozawa, R.; Hamaguchi, H. *Chem. Lett.* **2003**, *32*, 498−499.

(23) Holbrey, J. D.; Reichert, W. M.; Nieuwenhuyzen, M.; Johnston, S.; Seddon, K. R.; Rogers, R. D. *Chem. Commun*. **2003**, 1636−1637.

(24) Triolo, A.; Russina, O.; Arrighi, V., Juranyi, F.; Janssen, S.; Gordon, C. M. *J. Chem. Phys.* **2003**, *119*, 8549−8557.

(25) Berg, R. W.; Deetlefs, M.; Seddon, K. R.; Shim, I.; Thompson, J. M. *J. Phys. Chem. B* **2005**, *109*, 19018−19025.

(26) Umebayashi, Y.; Fujimori, T.; Sukizaki, T.; Asada, M.; Fuji, K.; Kanzaki, R.; Ishiguro, S. *J. Phys. Chem. A* **2005**, *109*, 8976−8982.

(27) Meng, Z.; Dölle, A.; Carper W. R. *J. Mol. Struct.* **2002**, *585*, 119−128.

(28) Morrow, T. I.; Maginn, E. J. *J. Phys. Chem. B* **2002**, *106*, 12807−12813.

(29) Katsyuba, S. A.; Dyson, P. J.; Vandyukova, E. E.; Vidiš, A. *Helv. Chim. Acta* **2004**, *87*, 2556−2565.

(30) Talaty, E. R.; Raja, S.; Shorthaug, V. J.; Dölle, A.; Carper, W. R. *J. Phys. Chem. B* **2004**, *108*, 13177−13184.

(31) Tsuzuki, S; Tokuda, H; Hayamizu, K.; Watanabe, M. *J. Phys. Chem. B* **2005**, *109*, 1674−1684.

(32) Heimer, N. E.; Del Sesto, R. E.; Meng, Z.; Wilkes, J. S.; Carper W. R. *J. Mol. Liq.* **2006**, *124*, 84−95.

(33) Paulechka, Y. U.; Kabo, G. J.; Blokhin, A. V.; Vydrov, O. A.; Magee, J. W.; Frenkel, M. *J. Chem. Eng. Data* **2003**, *48*, 457−462.

(34) Liu, Z.; Huang, S.; Wang, W. *J. Phys. Chem. B* **2004**, *108*, 12978−12989.

(35) Del Popolo, M. G.; Voth, G. A. *J. Phys. Chem. B* **2004**, *108*, 1744−1752.

(36) Urahata, S. M.; Ribeiro, M. C. C. *J. Chem. Phys.* **2004**, *120*, 1855−1863.

(37) Fuller, J.; Carlin, R.T.; De Long, H.C.; Haworth, D. *J. Chem. Soc., Chem. Commun*. **1994**, 299−300.

(38) Choudhury, A. R.; Winterton, N.; Steiner, A.; Cooper, A. I.; Johnson, K. A. *J. Am. Chem. Soc.* **2005**, *127*, 16792−16793.

(39) Suarez, P. A. Z.; Einloft, S.; Dullius, J. E. L.; de Souza, R. F.; Dupont, J. *J. Chim. Phys.* **1998**, *95*, 1626−1639.

(40) Kuhn, N.; Walker, M.; Steimann, M. *Z. Naturforsch., B: Chem. Sci.* **2002**, *57*, 248−250.

(41) (a) Frisch, M. J.; Trucks, G. W.; Schlegel, H. B.; Scuseria, G. E.; Robb, M. A.; Cheeseman, J. R.; Zakrzewski, V. G.; Montgomery, J. A.; Stratmann, R. E.; Burant, J. C.; Dapprich, S.; Millam, J. M.; Daniels, A. D.; Kudin, K. N.; Strain, M. C.; Farkas, O.; Tomasi, J.; Barone, V.; Cossi, M.; Cammi, R.; Mennucci, B.; Pomelli, C.; Adamo, C.; Clifford, S.; Ochterski, J.; Petersson, G.A.; Ayala, P.Y.; Cui, Q.; Morokuma, K.; Malick, D. K.; Rabuck, A. D.; Raghavachari, K.; Foresman, J. B.; Cioslowski, J.; Ortiz, J. V.; Stefanov, B. B.; Liu, G.; Liashenko, A.; Piskorz, P.; Komaromi, I.; Gomperts, R.; Martin, R. L.; Fox, D. J.; Keith, T.; Al-Laham, M. A.; Peng, C. Y.; Nanayakkara, A.; Gonzalez, C.; Challacombe, M.; Gill, P. M. W.; Johnson, B. G.; Chen, W.; Wong, M. W.; Andres, J. L.; Head-Gordon, M.; Replogle, E. S.; Pople, J. A. *Gaussian 98* (Revision A.2), Gaussian, Inc., Pittsburgh, Pa., USA, 1998. (b) Frisch, M. J.; Trucks, G. W.; Schlegel, H. B.; Scuseria, G. E.; Robb, M. A.; Cheeseman, J. R.; Montgomery, J. A.;. Vreven, Jr. T; Kudin, K. N.; Burant, J. C.; Millam, J. M.; Iyengar, S. S.; Tomasi, J.; Barone, V.; Mennucci, B.; Cossi, M.; Scalmani, G.; Rega, N.; Petersson, G. A.; Nakatsuji, H.; Hada, M.; Ehara, M.; Toyota, K.; Fukuda, R.; Hasegawa, J.; Ishida, M.; Nakajima, T.; Honda, Y.; Kitao, O.; Nakai, H.; Klene, M.; Li, X.; Knox, J. E.; Hratchian, H. P.; Cross, J. B.; Adamo, C.; Jaramillo, J.; Gomperts, R.; Stratmann, R. E.; Yazyev, O.; Austin, A. J.; Cammi, R.; Pomelli, C.; Ochterski, J. W.; Ayala, P. Y.; Morokuma, K.; Voth, G. A.; Salvador, P.; Dannenberg, J. J.; Zakrzewski, V. G.; Dapprich, S.; Daniels, A. D.; Strain, M. C.; Farkas, O.; Malick, D. K.; Rabuck, A. D.; Raghavachari, K.; Foresman, J. B.; Ortiz, J. V.; Cui, Q.; Baboul, A. G.; Clifford, S.; Cioslowski, J.; Stefanov, B. B.; Liu, G., Liashenko, A.; Piskorz, P.; Komaromi, I.; Martin, R. L.; Fox, D. J.; Keith, T.; Al-Laham, M. A.; Peng, C. Y.; Nanayakkara, A.; Challacombe, M.; Gill, P. M. W.; Johnson, B.; Chen, W.; Wong, M. W.; Gonzalez, C.; Pople, J. A. *Gaussian 03*, (Revision B.05), Gaussian, Inc., Wallingford CT, 2004.

(42) Becke, A. D. *J. Chem. Phys.* **1993**, *98*, 5648−5652.

(43) Lee, C.; Yang, W.; Parr, R. G. *Phys. Rev.* **1988**, *B37*, 785−789.

(44) (a) Sipachev, V. A. *J. Mol. Structure* **2001**, *67*, 567. (b) Sipachev, V. A. *Struct. Chem*. **2000**, *2/3*, 167.

(45) (a) Rauhut, G.; Pulay, P. *J. Phys. Chem.* **1995**, *99*, 3093−3100. (b) Rauhut, G.; Pulay, P. *J. Am. Chem. Soc.* **1995**, *117*, 4167−4172.

(46) Baker, J.; Jarzecki, A.; Pulay, P. *J. Phys. Chem. A* **1998**, *102*, 1412−1424.

(47) Katsyuba, S. A.; Grunenberg, J.; Schmutzler, R. *J. Mol. Struct.* **2001**, *559*, 315−320.

(48) Katsyuba, S. A.; Vandyukova, E. E. *Chem. Phys. Lett.* **2003**, *377*, 658−662.

(49) (a) Cancès, M. T.; Mennucci, B.; Tomasi, J. *J. Chem. Phys.* **1997**, *107*, 3032−3041. (b) Cossi, M.; Barone, V.; Mennucci, B.; Tomasi, J. *Chem. Phys. Lett.* **1998**, *286*, 253. (c) Mennucci, B.; Tomasi, J. *J. Chem. Phys.* **1997**, *106*, 5151−5158. (d) Cossi, M.; Scalmani, G.; Rega, N.; Barone, V. *J. Chem. Phys.* **2002**, *117*, 43−54.

(50) Iogansen, A. V. *Spectrochim. Acta, Part A* **1999**, *55*, 1585−1612.

(51) Katsyuba, S. A.; Schmutzler, R.; Grunenberg, J. *Dalton Trans.* **2005**, 1701−1706.

(52) Nama, D.; Kumar, P. G. A.; Pregosin, P. S.; Geldbach, T. J.; Dyson, P. J. *Inorg. Chim. Acta*, **2006**, *359*, 1907−1911.

(53) Heyns, A.M. *Spectrochim. Acta, Part A* **1977**, *33A*, 315−322.

(54) Kittel, C. *Introduction to Solid State Physics*, 8th ed.; Wiley & Sons, New York, 2005.

(55) (a) Katritzky, A. R.; Jain, R.; Lomaka, A.; Petrukhin, R.; Karelson, M.; Visser, A. E.; and Rogers, R. D. *J. Chem. Inf. Comput. Sci*. **2002**, *42*, 225. (b) Eike, D. M.; Brennecke, J. F.; Maginn, E. J. *Green Chem.* **2003**, *5*, 323−328.. Trohalaki, S.; Pachter, R. *QSAR Comb. Sci.* **2005**, *24*, 485.

(56) Feynman, R. P. *Statistical Mechanics: A Set of Lectures by R. P. Feynman*; Addison-Wesley: Reading, MA, 1998; pp 53−55.

(57) Further treatment of eq 3 is based mainly on the paper by Askadskii, A. A.; Matveev, Yu. I.; Slonimskii G. L.; Korshak, V. V. *Dokl. Akad. Nauk SSSR*, **1978**, *238*, 592.